

This discussion paper is/has been under review for the journal Geoscientific Model Development (GMD). Please refer to the corresponding final paper in GMD if available.

The chemical transport model Oslo CTM3

**O. A. Søvde¹, M. J. Prather², I. S. A. Isaksen^{1,3}, T. K. Berntsen^{1,3}, F. Stordal³,
X. Zhu², C. D. Holmes², and J. Hsu²**

¹Center for International Climate and Environmental Research – Oslo (CICERO),
Oslo, Norway

²Department of Earth System Science, University of California Irvine, California, USA

³Department of Geosciences, University of Oslo, Oslo, Norway

Received: 16 May 2012 – Accepted: 29 May 2012 – Published: 19 June 2012

Correspondence to: O. A. Søvde (asovde@cicero.uio.no)

Published by Copernicus Publications on behalf of the European Geosciences Union.

Title Page

Abstract

Introduction

Conclusions

References

Tables

Figures

◀

▶

◀

▶

Back

Close

Full Screen / Esc

Printer-friendly Version

Interactive Discussion



Abstract

We present here the global chemical transport model Oslo CTM3, an update of the Oslo CTM2. The update comprises a faster transport scheme, an improved wet scavenging scheme for large scale rain, updated photolysis rates and a new lightning parameterization. Oslo CTM3 is better parallelized and allows for stable, large time steps for advection, enabling more complex or high resolution simulations. Thorough comparisons between the Oslo CTM3, Oslo CTM2 and measurements are performed, and in general the Oslo CTM3 is found to reproduce measurements well. Inclusion of tropospheric sulfur chemistry and nitrate aerosols in CTM3 is shown to be important to reproduce tropospheric O₃, OH and the CH₄ lifetime well. Using the same meteorology to drive the two models, shows that some features related to transport are better resolved by the CTM3, such as polar cap transport, while features like transport close to the vortex edge are resolved better in the Oslo CTM2 due to its required shorter transport time step. The longer transport time steps in CTM3 result in larger errors e.g. near the jets, and when necessary, this can be remedied by using a shorter time step. An additional, more accurate and time consuming, treatment of polar cap transport is presented, however, both perform acceptably. A new treatment of the horizontal distribution of lightning is presented and found to compare well with measurements. Vertical distributions of lightning are updated, and tested against the old vertical distribution. The new profiles are found to produce more NO_x in the tropical middle troposphere, and less at the surface and at high altitudes.

1 Introduction

The University of Oslo chemistry-transport model, Oslo CTM2, has been used extensively over the past decade for studies of stratospheric and tropospheric chemistry, greenhouse gases, and climate forcing (Wild et al., 2003; Gauss et al., 2003; Berglen et al., 2004; Isaksen et al., 2005; Gauss et al., 2006; Dalsøren et al., 2007; Solberg

GMDD

5, 1561–1626, 2012

Oslo CTM3

O. A. Søvde et al.

Title Page

Abstract

Introduction

Conclusions

References

Tables

Figures



Back

Close

Full Screen / Esc

Printer-friendly Version

Interactive Discussion



et al., 2008; Søvde et al., 2008; Hoor et al., 2009; Dalsøren et al., 2010; Søvde et al., 2011a; Myhre et al., 2011; Hodnebrog et al., 2011). CTM2 was derived from a collaboration between Oslo and the University of California Irvine (UCI) in which the UCI development of CTMs (Prather et al., 1987; Hall and Prather, 1993, 1995) was combined with the Oslo development of forecast meteorology fields from the European Centre for Medium-Range Weather Forecasts (ECMWF) (Sundet, 1997). The Oslo CTM2 was first documented in Jonson et al. (2001). Since CTM2, the core CTM has developed more efficient transport methods and diagnostics (Prather et al., 2008, 2011) and more accurate simulation of atmospheric processes, such as photolysis and scavenging, based on the ECMWF forecast data (Neu et al., 2007; Neu and Prather, 2012). These developments have been merged with CTM2's stratosphere-plus-troposphere, gas-plus-aerosol, chemistry model to form the Oslo CTM3, which is documented and evaluated here.

Overall, CTM3 retains most of the capabilities of CTM2, but has increased computational efficiency, thus enabling much higher resolution or multi-year ensemble/sensitivity simulations. CTM3 also has improved the representation of sub-grid processes such as convection, scavenging, and fractional cloud cover. CTM3 is stable for much longer time steps than is CTM2, but this does increase the transport error (Prather et al., 2008).

Section 2 describes the new components of Oslo CTM3, noting the main differences from CTM2. We focus on transport and the gas-phase chemistry components, so our simulations will also include aerosol modules that affect chemistry directly. Available aerosol modules currently in CTM2 (e.g., Grini et al., 2002; Berglen et al., 2004; Grini et al., 2005; Myhre et al., 2006) will be evaluated in a second aerosol-focused paper (Søvde et al., 2012). Section 3 evaluates the new model against some traditional chemistry climatologies and new observational case studies. We show that the inclusion of the tropospheric sulfur cycle (Berglen et al., 2004) and nitrate aerosols (Myhre et al., 2006), which directly affect the chemistry, has become more important in CTM3 than in

Oslo CTM3

O. A. Søvde et al.

[Title Page](#)

[Abstract](#)

[Introduction](#)

[Conclusions](#)

[References](#)

[Tables](#)

[Figures](#)



[Back](#)

[Close](#)

[Full Screen / Esc](#)

[Printer-friendly Version](#)

[Interactive Discussion](#)



CTM2. Some sensitivity studies are presented in Sect. 4, while Sect. 5 concludes the study.

2 Model description

The Oslo CTM3 is a global 3-D CTM, driven by 3-hourly meteorological forecast data from the European Centre for Medium-Range Weather Forecasts (ECMWF) Integrated Forecast System (IFS) model, produced on a daily basis with 12 h of spin-up starting from an analysis at noon on the previous day, which are then pieced together to give a uniform dataset for a whole year. Winds, temperature, pressure and humidity are given as instantaneous values every 3 h, while other variables such as rainfall and convective fluxes are averages over the 3-h interval. The cycle used here is 36r1, starting from ERA-Interim analyses.

The full vertical resolution of the IFS (60 layers) is used in CTM3. The resolution near the tropical tropopause is ~ 1 km, and the uppermost, 10-km thick layer is centered at 0.11 hPa (about 60 km). A horizontal Gaussian-grid of resolution T42 ($\sim 2.8^\circ \times \sim 2.8^\circ$) is the standard resolution of CTM3, but the original resolution of the IFS (T319L60, $\sim 0.5^\circ \times \sim 0.5^\circ$) can be also be used. The UCI/Oslo CTM framework is flexible and can be used on any 3-D quadrilateral grid.

In general, when moving from CTM2 to CTM3, there are no changes in the chemistry and aerosol modules, and the CTM2 literature still applies. Some changes are inevitable due to the new core, e.g. the new wet scavenging, and in this Section we describe these changes. The main model improvements are listed in Table 1, and will be discussed in this Section: transport (Sect. 2.2), scavenging (Sect. 2.3), calculation of photodissociation rates (Sect. 2.4) and lightning NO_x (Sect. 2.6). First, we give a short introduction to the chemistry and aerosol schemes applied.

Title Page

Abstract

Introduction

Conclusions

References

Tables

Figures



Back

Close

Full Screen / Esc

Printer-friendly Version

Interactive Discussion



2.1 Chemistry

The chemistry of CTM3 is identical to CTM2, which has been described in earlier work, comprising comprehensive schemes for both tropospheric and stratospheric chemistry. Tropospheric chemistry was introduced by Berntsen and Isaksen (1997), stratospheric chemistry is based on Stordal et al. (1985), and the tropospheric sulfur chemistry is described by Berglen et al. (2004). The use of full tropospheric and stratospheric chemistry has been reported by e.g., Gauss (2003), Søvde et al. (2008) and Søvde et al. (2011b).

The tropospheric scheme is a stand-alone module, while the stratospheric module requires tropospheric chemistry to be included. Having the option to turn off stratospheric chemistry is preferable due to computational limits and when the lower troposphere is the domain of interest. In such cases, stratospheric losses of species are calculated based on approximate lifetimes, except for stratospheric O_3 and NO_x , which are set from climatological values. The CTM2 climatology has recently been revised to a multi-year model climatology of O_3 and NO_x (Skeie et al., 2011), however, this will not be described here.

In this work, we focus on gas phase chemistry. However, as will be described, we also carry out simulations where we in addition include aerosol modules which affect chemistry directly. These are the tropospheric sulfur module comprising sulfur chemistry and sulfate aerosols (Berglen et al., 2004), and nitrate aerosols (Myhre et al., 2006), which affect gaseous HNO_3 . The latter also requires sea salt aerosols to be included (Grini et al., 2002). As already noted, these are unchanged from CTM2 to CTM3, and we will not evaluate the aerosols here, that is left for a separate study.

2.2 Transport

The model transport covers large scale advection treated by the second order moments (SOM) scheme (Prather, 1986), convective transport based on Tiedtke (1989)

GMDD

5, 1561–1626, 2012

Oslo CTM3

O. A. Søvde et al.

Title Page

Abstract

Introduction

Conclusions

References

Tables

Figures



Back

Close

Full Screen / Esc

Printer-friendly Version

Interactive Discussion



and boundary layer mixing based on Holtslag et al. (1990). The latter is the same in both Oslo CTM3 and Oslo CTM2, and will not be described further.

2.2.1 Advection

In the Oslo CTM3 we have implemented the UCI CTM transport core documented by Prather et al. (2008) (P2008 from now). This new core advection scheme (P2008) is a significant advance in terms of computational efficiency and flexibility compared with the original SOM method used in CTM2 (Prather, 1986).

The 3-D advection is isotropic, i.e. it uses the same SOM algorithm in all dimensions. The zonal (U) and meridional (V) meteorological fields (3-h instant values) are used to compute the vertical (W) field. The CTM keeps and computes only dry-air fluxes, masses and surface pressures. Small inconsistencies in the pressure tendency compared with the convergence fields from $[U] + [V]$ are corrected by small adjustments (typically $<1\%$) in $[U]$ and $[V]$ to ensure consistent mass fields (i.e. the dry-air mass is conserved and never changed except by resolved advective transport). Convection is diagnosed as updrafts and downdrafts separately, taking both entrainment and detrainment into account (see Sect. 2.2.2). The inferred residual subsidence (i.e. a W -like flux) is combined with the large-scale $[W]$ from the $[U] + [V]$ fields to eliminate one advection step.

Advection in each dimension is calculated as a pipe-flow as in P2008, wherein each pipe calculates its own CFL limit (i.e. flux out of a grid box cannot exceed 99% of the mass) and then if a reduced time step is required, each pipe does multi-stepped advection internally saving large amounts of computational overhead and not requiring the global calculation to slow down for enhanced multi-stepping in the jet regions. The global advection time step, no longer limited by the CFL criteria, is now limited by the Lifshitz criteria, which is implemented here by requiring that during the sequence of advection, $[\text{Convection} + W] + [U] + [V]$, the mass of any grid box does not fall below 5% of its initial value. This new CTM3 core advection allows for dynamical time steps as large as 45 min for T42L60 ($\sim 2.8^\circ$) fields and 15 min for T319L60 ($\sim 0.55^\circ$) fields,

Title Page

Abstract

Introduction

Conclusions

References

Tables

Figures



Back

Close

Full Screen / Esc

Printer-friendly Version

Interactive Discussion



Oslo CTM3

O. A. Søvde et al.

[Title Page](#)[Abstract](#)[Introduction](#)[Conclusions](#)[References](#)[Tables](#)[Figures](#)[Back](#)[Close](#)[Full Screen / Esc](#)[Printer-friendly Version](#)[Interactive Discussion](#)

demonstrating the advantage of being Lifshitz-limited for high-resolution CTMs. In contrast to this, the Oslo CTM2 use the same time step at low and high latitudes, and therefore combined high-latitude gridboxes (so-called extended polar zones) during transport, to avoid very short global time steps. The averaging itself made the treatment less optimal for polar studies, as is shown in P2008 and later in this work.

The over-the-pole flow in P2008 worked well for typical solid-body rotation tests (Williamson et al., 1992), but recently we found that under certain conditions it fails dramatically. First is the blob of high-N₂O air in the middle stratosphere that splits off from the tropics in March 2005 and survives into August (Manney et al., 2006). Second is the Arctic ozone hole of 2011 in which very low O₃ columns (320 DU vs. 450 DU) are maintained through March and into early April. In both cases an isolated vortex (anti-cyclonic in the first, and cyclonic in the second) has an edge at the pole, and in both cases the P2008 polar advection algorithm shredded the vortex. With these two test cases, a new over-the-pole treatment was developed.

The P2008 connection of the two over-the-pole, pie-shaped grid boxes at their vertices was severed (i.e. zero mass flux between the boxes) and all polar flow is now forced through the $[U]$ fields at the next-to-pole latitude circle. For the ECMWF forecast fields, these winds are smooth and appear to accurately describe the edge of the vortex at the pole. This new algorithm is denoted here as V2, and the case study of the N₂O blob is discussed below. One problem with V2 is that the amount of air forced through the polar pie-shaped boxes is large and the Lifshitz limiter requires much shorter time steps (e.g. 15–20 min). The final algorithm for CTM3 reduces the resolution at the poles but maintains the smooth, vortex-preserving flow: For $[U]$ and $[V]$ advection the polar box is concatenated with its lower-latitude neighbor, preserving all moment information; advection is calculated; and then the combined polar boxes are remapped onto the basic grid using the moments.

The V2 transport may change the global time step required for transport, or it may change the internal 1-D transport pipe time step. A shorter global time step generally makes the transport more accurate, increasing the overall computing time, while

2.3 Scavenging

Scavenging covers dry deposition, i.e. uptake by soil or vegetation at the surface, and washout by convective and large scale rain. Dry deposition is in principle unchanged from CTM2 to CTM3 (Wesely, 1989). However, the CTM3 uses a more detailed land use dataset, which produce slightly different deposition values. While CTM2 uses 5 categories only, the CTM3 land use is taken from the 18-category ISLSCP2 MODIS dataset (the simpler ISLSCP88 with 9 categories is also available).

In general, the amount of tracer solved in rain is calculated using Henry's Law. For very soluble species, such as HNO_3 , it is often assumed that all is solved. Also, rain falling into drier air will experience evaporation.

The CTM2 large scale wet scavenging assumes that the gridbox fraction subject to rain (f) is

$$f = c_f \frac{\text{net rain out}}{\text{cloud water} + \text{ice}} \quad (2)$$

where c_f is cloud fraction and net rain out is the difference between outgoing (grid box bottom) and incoming (top) rain. If net rain out is larger than the available cloud water + ice, CTM2 assumes $f = c_f$. Then the amount solved, either from Henry's law or the whole gridbox fraction, is calculated and transported downwards. Evaporation is based on a similar approach, and occurs only when rain into the gridbox is larger than rain out of the grid box.

CTM3 also uses Henry's Law to calculate the solution of species in rainfall, but has a more complex cloud model that accounts for overlapping clouds and rain (Neu and Prather, 2012). The updated scheme also covers HNO_3 removal on ice, calculated according to Kärcher and Voigt (2006) for temperatures below 258 K. For $258 \text{ K} < T < 273 \text{ K}$, the uptake is modified by a retention coefficient.

Convective scavenging (Berglen et al., 2004) is unchanged from CTM2 to CTM3, and therefore treats convective precipitation as rain. Splitting it into ice and liquid is

Title Page

Abstract

Introduction

Conclusions

References

Tables

Figures



Back

Close

Full Screen / Esc

Printer-friendly Version

Interactive Discussion



beyond the scope of this work. However, due to the new model structure there are some differences in the amounts removed by convective precipitation.

We will diagnose wet scavenging more closely in Sect. 3.4.

2.4 Photodissociation

5 For calculation of photodissociation rates, the fast-J2 (Bian and Prather, 2002) in CTM2 has been replaced by fast-JX (Prather, 2009) in CTM3. The differences between fast-J2 and fast-JX are not tested directly here; fast-JX is treated as a part of the model core update.

10 An important update connected to fast-JX is the new cloud overlap treatment, described by Neu et al. (2007). The only difference from their original treatment is that instead of using multiple cloud profiles in one gridbox column, a single cloud profile is picked randomly from the possible profiles. This will be explained below.

15 The fast-JX scheme version 6.5 calculates photolysis rates (J's) for stratospheric and tropospheric species from the surface to 60 km for a single column atmosphere defined by CTM layers that can contain both absorbers (O_2 , O_3 , aerosols) and scatterers (molecules (Rayleigh), aerosols, cloud liquid water, cloud ice water). Based on new data, solar fluxes were revised upward in the 180–240 nm region and thus photolysis of O_2 increased, resulting in CTM3 showing better agreement with observed O_3 in the stratosphere. Cross sections and quantum yields are as described by Hsu and Prather
20 (2009), using photochemistry rates from Sander et al. (2006) and cross sections from Atkinson et al. (2004). Photolysis of volatile organic compounds (VOC) is taken solely from the latter, and uses individually tuned Stern-Vollmer pressure dependencies for the quantum yields. With the JPL-2010 update that also includes most VOCs Sander et al. (2011) and more complex wavelength-pressure dependence, the next release
25 of fast-JX (version 6.7) has a new approach for handling the Stern-Vollmer pressure dependence of the VOC quantum yields. The combined cross section plus quantum yield tables for the fast-JX wavelength bins are calculated for three troposphere temperatures with their included pressures for a typical lapse rate: 295 K (0 km, 1000 hPa),

Title Page

Abstract

Introduction

Conclusions

References

Tables

Figures



Back

Close

Full Screen / Esc

Printer-friendly Version

Interactive Discussion



272 K (5 km, 566 hPa), 220 K (13 km, 178 hPa). Interpolation is done across temperature as before.

The multi-stream scattering calculation assumes horizontally uniform layers. The J-values are generally computed at the mid-point of each layer with the flux divergence computed between the top and bottom of each layer. When optically thick clouds occur, extra points are inserted within each CTM layer using a logarithmic scale to more accurately (and efficiently) calculate the average J-values throughout the layer.

When cloud fractions are specified for a grid box, an algorithm (Neu et al., 2007) groups the cloudy layers into maximally overlapping connected layers and randomly overlapping groups. This choice can then be used to define a number of independent, single column atmospheres, each with a fractional area. For the T42L60 fields here, the number of single column atmospheres in a box can be quite large, and is truncated to be no more than 20 000 by forcing maximal overlapping clouds in the upper layers. In Neu et al. (2007) calculation of average J's over the box is done by quadrature: the fractional areas of nearly clear (cloud optical depth < 0.5), hazy (cirrus), thick (stratus), and opaque (cumulus) are calculated and a sample column atmosphere from each type is selected to represent that region (i.e., J's are weighted by the fractional area of that type). Using the fractional cloud statistics from the T42L60 fields here, the number of calls to fast-JX averages 2.8 per grid box (out of a maximum of 4).

To reduce this computational cost, a new approach is taken in CTM3, whereby a single column atmosphere is chosen randomly using its fractional area as the likelihood of being selected. The random selection is controlled and repeatable, being generated from a fixed, prime-number (10 007) sequence of random numbers. For each three-hourly averaged statistics of cloud water and fraction, three randomly sampled single atmospheres are chosen and held fixed for 1 h. This new random cloud-fraction algorithm has been tested against the quadrature method in the UCI CTM and found to produce results (e.g., tropospheric O₃, OH) from five parallel simulations starting with different random seeds that cluster about the quadrature method. All of these results differ clearly from the fast-J2 (CTM2) average cloud fraction approach in which there is

[Title Page](#)

[Abstract](#)

[Introduction](#)

[Conclusions](#)

[References](#)

[Tables](#)

[Figures](#)



[Back](#)

[Close](#)

[Full Screen / Esc](#)

[Printer-friendly Version](#)

[Interactive Discussion](#)



never direct sunlight at the surface for boxes with any fractional clouds (see Neu et al., 2007).

In this work, CTM3 uses a climatology for atmospheric black carbon in the fast-JX calculations. This will be revised when all CTM2 aerosol modules have been included into the CTM3.

2.5 Emissions

In this work, the model surface emissions are taken from RETRO year 2000 (RETRO emissions, 2006), using diurnal variations for industrial emissions. NO_x emissions are emitted as 96 % NO and 4 % NO_2 as in Oslo CTM2, to account for unresolved plume processes.

Biomass burning, however, is taken from the Global Fires Emission Database version 3 (GFEDv3), scaled to a height distribution available from RETRO. We use monthly mean GFEDv3 data for the years 1997–2010, and we match the emissions to the meteorological year in the model. NO_x emissions are emitted assuming nitrogen content to be 90 % as NO and 10 % as NO_2 .

Aircraft emissions are taken from QUANTIFY, for the year 2000 (Owen et al., 2010), and are emitted as NO. No plume processes are parameterized; the CTM2 plume model was left out of this study because it was tailored to a lower resolution and hence no longer appropriate.

Lightning NO_x emissions are described in Sect. 2.6, and change daily and yearly according to the meteorological year.

As the main purpose for this study is to document the Oslo CTM3, we keep the current emission setup with surface and aircraft emissions fixed at 2000 level. Recently more updated datasets have become available, e.g., Lamarque et al. (2010), but we will leave this for later studies.

Title Page

Abstract

Introduction

Conclusions

References

Tables

Figures



Back

Close

Full Screen / Esc

Printer-friendly Version

Interactive Discussion



2.6 Lightning NO_x

Lightning NO_x (L-NO_x) emissions in the model depend on the convective mass flux in each model column, which are available from the meteorological input data. L-NO_x is emitted as NO, however, the treatment has changed from CTM2 to CTM3.

While the CTM2 scheme is described by Berntsen and Isaksen (1999), the Oslo CTM3 uses a recently updated L-NO_x scheme from from the UCI CTM. In the latter the geographical L-NO_x distribution is generated by scaling the Price and Rind (1992) equations with to match lightning flash rates observed by Optical Transient Detector (ODT, Christian et al., 1999a) and Lightning Imaging Sensor Christian et al. (LIS, 1999b).

L-NO_x emissions at a given time t are

$$E(\mathbf{x}, L, t) = \bar{f}(\mathbf{x}, t) \gamma v_L \quad (3)$$

where $\bar{f}(\mathbf{x}, t)$ is the grid-averaged lightning flash rate at the horizontal location \mathbf{x} and time t , γ is the NO_x yield per flash (246 molflash⁻¹), and v_L is the vertical distribution of emissions at model level L .

Lightning is diagnosed in the Oslo CTM3 when convection out of the boundary layer exceeds a grid-averaged updraft velocity of 0.01 ms⁻¹ at ~850 hPa. In addition, the surface must be warmer than 273K and the cloud top colder than 233K to support charge separation within the cloud (Williams, 1985).

When these conditions are met, the in-cloud flash rate (f) has the same functional dependence on cloud-top height $H(\mathbf{x}, t)$ as in Price and Rind (1992):

$$f(\mathbf{x}, t) = \begin{cases} \alpha_l H(\mathbf{x}, t)^{4.9} & \text{over land} \\ \alpha_o H(\mathbf{x}, t)^{1.73} & \text{over ocean} \end{cases} \quad (4)$$

We develop new scale factors, $\alpha_l = 3.44 \times 10^{-6} \text{ s}^{-1} \text{ km}^{-4.9}$ and $\alpha_o = 2.24 \times 10^{-3} \text{ s}^{-1} \text{ km}^{-1.73}$, to match the climatological flash rates over land and ocean,

Title Page

Abstract

Introduction

Conclusions

References

Tables

Figures



Back

Close

Full Screen / Esc

Printer-friendly Version

Interactive Discussion



35 s⁻¹ and 11 s⁻¹, respectively. The factors are calculated for our meteorological data over 1999–2009 (ECMWF cycle 36r1, resolution T42L60), constrained by OTD-LIS observations during 1995–2005. These coefficients differ from those reported by Price and Rind (1992) by up to a factor of 10, and must be re-calibrated for different resolutions, e.g. T319.

Convective fluxes and the clouds that contain them occupy a small fraction of the horizontal area of a model grid square. Therefore, lightning also occupies a small fraction of the model grid area. The grid-averaged lightning flash rate (\bar{f}) is then

$$\bar{f}(\mathbf{x}, t) = a(\mathbf{x}, t) f(\mathbf{x}, t). \quad (5)$$

where a , the area fraction experiencing lightning, is estimated as a weighted average of the cloud fractions in the column:

$$a(\mathbf{x}, t) = \frac{\sum_{l=1}^{l_t} f_{c,l} w_l}{\sum_{l=1}^{l_t} w_l}. \quad (6)$$

Here, $f_{c,l}$ is the cloudy fraction at level l , w_l is the wet convective mass flux at level l , and l_t is the model level at the cloud top.

With the yield per flash of 246 mol flash⁻¹, or equivalently $\gamma = 3.45$ kg (N) per flash, we impose mean climatological L-NO_x emissions of 5 Tg (N) yr⁻¹.

The model distributes NO_x emissions vertically through the convective column according to observed profiles (Ott et al., 2010) for 4 world regions. These profiles are scaled vertically to match the height of each convective plume in the CTM and already account for vertical mixing of lightning NO_x within the cloud. Geographic region definitions are from Allen et al. (2010) and Murray et al. (2011).

Between CTM2 and CTM3, as shown in Fig. 1, there are small differences in the annual mean flash rates. Lightning over ocean in CTM3 spreads over smaller areas than in CTM2, but still cover larger areas than observed. This is most pronounced around Indonesia, however, the differences are small in absolute terms.

Title Page

Abstract

Introduction

Conclusions

References

Tables

Figures



Back

Close

Full Screen / Esc

Printer-friendly Version

Interactive Discussion



Lightning flashes in CTM3 are reduced over South America compared to CTM2, and are still too small over Africa. However, the standard deviations in these areas, based on monthly mean flash rates, are more realistic in CTM3. There is still too much lightning at high latitudes in Canada and Eurasia, even though the absolute values are small.

As already noted, the differences between CTM2 and CTM3 are in general small, however, high flash rates are better modelled in CTM3, which has the benefit that it is closely tied to observational constraints (Price and Rind, 1992), rather than the product of mass flux and cloud-top-height.

The CTM2 L-NO_x scheme is not tested in the CTM3, however, we present in Sect. 4 a CTM3 sensitivity study where the CTM2 vertical distribution (Pickering et al., 1998) is applied and compared to a simulation using the new vertical distribution (Ott et al., 2010). It has, however, not been possible to disentangle the differences induced by the different horizontal distributions in CTM2 and CTM3.

3 Evaluation

The Oslo CTM3/UCI CTM transport is evaluated in Prather et al. (2008). Here we evaluate the Oslo CTM3 against the Oslo CTM2 and measurements. The comparison is carried out in two steps, focusing first on the stratosphere and then on the troposphere.

For this study, we have carried out several full transport-chemistry simulations, listed in Table 2. Also listed are the time spans simulated for the different runs.

The main runs are C3, C3_NIT, C2 and C2_NIT, and the others are sensitivity studies. The NIT-simulations include sulfur chemistry (Berglen et al., 2004), sea salt aerosols (Grini et al., 2002) and nitrate aerosols (Myhre et al., 2006). As will be explained, the C3 simulation produce higher tropospheric OH and O₃ than C2, due to less removal by wet scavenging (e.g. HNO₃ and H₂O₂) and more active photochemistry. This motivated the inclusion of the NIT studies, which were known to reduce OH. Comparisons with

Title Page

Abstract

Introduction

Conclusions

References

Tables

Figures



Back

Close

Full Screen / Esc

Printer-friendly Version

Interactive Discussion



observations will in general be made with C3_NIT and C2_NIT, although we will also comment on C3 and C2.

The sensitivity studies are all without sulfur and nitrate aerosols, and are compared with C3. C3_30MIN is the C3 run with an operator split time step of 30 min, which is half of that in C3, and C3.V2 is the C3 run with the more accurate polar cap treatment described in Sect. 2. C3_PIC tests the CTM2 vertical lightning NO_x distribution in CTM3, presented in Sect. 4.

For the main runs, the simulated period is 1997–2005, while the other runs are 14-months simulations starting from the instant C3 field at 1 November 2004. The first year (1997) was started from an already spun-up simulation, more specifically from an instant snapshot of all species at 1 January 2005, and should therefore be considered as spin-up. The year 2005 was chosen because the Northern Hemisphere meteorological conditions were somewhat similar to 1997.

3.1 Stratosphere

For the evaluation of the stratosphere, we first consider the stratospheric age of air and how the age tracers differ from CTM2 to CTM3. In addition, we carry out comparisons with satellite measurements.

3.1.1 Age of air

The UCI CTM/Oslo CTM3 stratospheric age of air was presented by Prather et al. (2008). To compare the CTM3 with CTM2, we calculate the stratospheric age of air from an age spectrum tracer, increasing linearly in the tropical troposphere (Hall et al., 1999). The age is calculated for T42 horizontal resolution, and the runs are listed in Table 3.

Simulations of 20 years were carried out using 2005 meteorology recycled annually, and age of air was calculated from the linearly increasing source in the tropical troposphere. Note that the use of a tropical source gives greater north-south symmetry

[Title Page](#)

[Abstract](#)

[Introduction](#)

[Conclusions](#)

[References](#)

[Tables](#)

[Figures](#)



[Back](#)

[Close](#)

[Full Screen / Esc](#)

[Printer-friendly Version](#)

[Interactive Discussion](#)



Oslo CTM3

O. A. Søvde et al.

[Title Page](#)[Abstract](#)[Introduction](#)[Conclusions](#)[References](#)[Tables](#)[Figures](#)[Back](#)[Close](#)[Full Screen / Esc](#)[Printer-friendly Version](#)[Interactive Discussion](#)

in the lower stratosphere than from northernly-only sources used in observations, see Prather et al. (2011). Annual zonal means of age of air are shown in Fig. 2 for CTM3 and CTM2, with operator split time step of one hour (C3_AGE and C2_AGE), along with C3_AGE_30MIN where the time step is 30 min. In general, the maximum age value is slightly smaller in CTM3. However, the main difference between CTM3 and CTM2 can be found in the Southern Hemisphere for ages older than 4 yr, where the CTM2 produce a southward blob of younger air at around 40° S–70° S and 50 hPa–10 hPa altitude. This feature is not captured by C3_AGE, but is better captured in C3_AGE_30MIN, where the shorter operator split time step reduces the errors, especially around the polar jets (Prather et al., 2008). Between C3_AGE and C2_AGE, the maximum age difference in this region amounts to 0.67 yr, as shown in Fig. 3a. By halving the operator split time step as in C3_AGE_30MIN, the difference to C2_AGE is reduced to 0.29 yr (Fig. 3b).

Whereas a comparison of C3_AGE_30MIN against C3_AGE shows a noticeably improvement when reducing the time step (not shown), the improved polar cap transport (C3_AGE_V2) only changes the stratospheric age of air slightly (not shown).

From a latitude/longitude view, the difference between CTM2 and CTM3 at ~50 hPa (not shown) is found around the polar vortex edge, indicating that the vortices are more closed off in CTM2. Halving the time step removes most of this dissimilarity (Prather et al., 2008), consistent with the better resolved blob seen in Fig. 2c.

Even though the age is primarily a stratospheric diagnostic, the troposphere looks similar in both models, although poleward transport seem to be slightly faster in the CTM2 Southern Hemisphere troposphere. Section 3.2 will give better insight on the troposphere.

3.1.2 Comparisons with satellites

In Fig. 4 we show the interannual variability of the daily zonal mean O₃ column, from 1997 to 2005, where model results from CTM3 (C3_NIT) and CTM2 (C2_NIT) are

compared to Total Ozone Mapping Spectrometer (TOMS) instrument, available from <http://mirador.gsfc.nasa.gov/>.

Both models reproduce the total O₃ column well. Figure 4 shows clearly that the models are capable of producing reasonable polar O₃ loss, as previously reported (Søvde et al., 2008, 2011b; Balis et al., 2011). Other features that are driven by the meteorological dynamics and the seasonality of the amount of sunlight available, can also be seen, such as the Antarctic Ozone Hole split in 2002.

In general, the Oslo CTM3 and CTM2 O₃ columns agree well with TOMS in the Northern Hemisphere (NH). At Southern Hemisphere (SH) mid-latitudes, CTM3 is somewhat lower than observed and CTM2 seem to reproduce TOMS better, confirming the that CTM2 has a somewhat more closed-off polar vortex, and that the CTM3 transport errors are larger near the SH polar jet. In 2002, however, when the Antarctic O₃ hole was smaller and also split in two, the models are more similar at SH mid-latitudes. Comparing C3_NIT with C3 (not shown), shows that the largest differences in O₃ columns are at high latitudes in summer, most pronounced in SH. Similar, but smaller, differences is seen for C2_NIT vs C2.

The use of real meteorological data allows a more thorough comparison on a one-to-one basis. As an example, we show in Fig. 5 the daily average total O₃ column for 28 November 2000, when an O₃ mini-hole occurred over Europe (Semane et al., 2002). Both CTM3 (C3_NIT and C3) and CTM2 reproduce this event well and to a better degree than in Søvde et al. (2008), where 40-layer meteorological data was used.

It can be seen in Fig. 5 that the CTM2 produce almost uniform polar caps due to its transport treatment. CTM3, however, does not, and reproduce e.g. the Antarctic low-O₃ tongue at about 170° E to a better degree. In agreement with Fig. 4, the SH mid-latitude maximum is somewhat higher in Oslo CTM2. Similar features can be found in 2005 also, where we have found that this bias is reduced in C3_30MIN.

The Oslo CTM3 mostly produce higher column values than CTM2, the latter having a slightly lower stratospheric O₃. This is shown in Fig. 6, where the models are compared to Earth Observing System Microwave Limb Sounder (MLS) version 3.3

[Title Page](#)

[Abstract](#)

[Introduction](#)

[Conclusions](#)

[References](#)

[Tables](#)

[Figures](#)



[Back](#)

[Close](#)

[Full Screen / Esc](#)

[Printer-friendly Version](#)

[Interactive Discussion](#)



observational data (Froidevaux et al., 2008; Livesey et al., 2011). Zonal means for 30-degree latitude bands (60° for the tropics) are given for January 2005 and July 2005, with standard deviation shown as horizontal bars. CTM2 standard deviation is not shown; it is similar to CTM3. For O₃ (Fig. 6a), CTM3 (C3_NIT) reproduce MLS better than CTM2, due to the updated photolysis treatment. It should be noted that in the stratosphere, C3_NIT and C3 are only negligibly different, because their main differences are in the troposphere. Also the sensitivity studies C3_30MIN and C3_V2 produce negligibly different profiles (not shown).

In Fig. 6b we compare the models with MLS HNO₃ measurements (Santee et al., 2007; Livesey et al., 2011), where the CTM3 and CTM2 reproduce MLS well in summer but underestimates it at altitudes above 30 hPa in winter. The latter may be due to lack of nitrogen species transported downwards from the mesosphere (Randall et al., 2006, 2009), or the lack of in-situ NO_x sources caused by energetic particle precipitation (Jackman et al., 2008; Semeniuk et al., 2011) and conversion to HNO₃ by e.g. ion clusters (Verronen et al., 2008, 2011). Below 30 hPa the models do fairly well, also when it comes to the standard deviation. There are no big differences between CTM2 and CTM3, although CTM3 seems to perform slightly better in summer. Again, C3_V2 and C3_30MIN produce almost identical profiles, except the latter at SH high latitudes, where small differences up to 5% in HNO₃ can be seen (not shown).

Lastly, we compare modelled N₂O with MLS measurements (Lambert et al., 2007; Livesey et al., 2011), shown in Fig. 6c. CTM3 and CTM2 produce very similar N₂O, however, at all latitudes except high wintertime latitudes, both models underestimate N₂O between about 30 hPa and 1 hPa, indicating stagnant vertical transport in the meteorological data. An earlier cycle of meteorological data (cycle 29) shows slightly better comparison (not shown), which could indicate that cycle 36r1 has stagnant vertical transport. We will come back to this. Again there are negligible differences between C3_NIT, C3, C3_30MIN and C3_V2.

[Title Page](#)[Abstract](#)[Introduction](#)[Conclusions](#)[References](#)[Tables](#)[Figures](#)[Back](#)[Close](#)[Full Screen / Esc](#)[Printer-friendly Version](#)[Interactive Discussion](#)

3.1.3 Modelling a frozen-in Anti-Cyclone

An important change from CTM2 to CTM3 is the better polar transport treatment, and to demonstrate this we look at the 2005 Frozen-in Anti-Cyclone (FrIAC) in the Arctic reported by Manney et al. (2006) and more recently studied by Allen et al. (2011).

In Fig. 7 we show a Hovmöller plot, as in Allen et al. (2011), of N_2O at the altitude 850 K and latitude $78^\circ N$, for MLS measurements, the Oslo CTM3 and the Oslo CTM2. MLS measurements have been binned into $5 \times 5^\circ$ latitude/longitude bins, due to the sparsity of observations. N_2O from the CTMs were put out hourly in 3-D and interpolated to $78^\circ N$.

The Oslo CTM3 reproduces transport of N_2O well, although the amplitude is underestimated. Because the main difference between C3 and C3_NIT is in the troposphere, there are negligible differences between them. As shown in Fig. 6, N_2O was in general underestimated between 30 hPa and 1 hPa at most latitudes, which could explain the overall low N_2O abundances relative to observations in Fig. 7. This could render N_2O values too low even before entering the polar latitudes.

The Oslo CTM2 does not capture this transport well. Its transport pattern is similar to CTM3, but due to the averaging of the polar gridboxes, where the N_2O is smeared out, the values are substantially lower than for CTM3.

From sensitivity studies, we have found (but not shown) that halving the operator split time step (C3_30MIN) does not change the CTM3 performance in terms of the N_2O blob. This is mainly because the blob was located above the region where main transport differences between C3 and C3_30MIN are found.

However, the improved polar transport (C3_V2) produce up to 30 % more N_2O in the blob after 1 May. In general, the difference arise when large wind gradients are located across the combined grid boxes in CTM3 transport.

Studies involving polar cap transport and to some extent Arctic and Antarctic studies, will clearly benefit from using V2-transport, while other studies may benefit of the

Title Page

Abstract

Introduction

Conclusions

References

Tables

Figures



Back

Close

Full Screen / Esc

Printer-friendly Version

Interactive Discussion



shorter computing time achieved by combining polar boxes, and find its performance acceptable.

3.2 Troposphere

In this section we focus on the troposphere, describing transport differences between Oslo CTM3 and CTM2 and also compare the models with observations.

3.2.1 Transport in the troposphere

CTM3 and CTM2 are expected to differ slightly in the troposphere due to the differences in transport treatment. We have studied the linearly increasing age of air tracer for year 20, and in the zonal mean C3_AGE differs from C2_AGE by only $\sim 0.5\%$ between the surface and ~ 300 hPa (not shown). In general the CTM3 tropospheric mixing ratios are slightly higher south of 50° S, indicating slightly faster transport to southernmost latitudes. North of 50° S the differences are generally related to convective regions, where CTM2 has higher mixing ratio than CTM3 in the lower troposphere. This is mainly due to differences in entrainment and detrainment, and will be explained in Sect. 3.2.2.

3.2.2 Convective transport

Recently, Hoyle et al. (2011) presented convective tracer transport using different CTMs, among them the Oslo CTM2, using a different set of meteorological data than used here. To compare the differences in transport between Oslo CTM3 and CTM2, we do similar tracer studies with one tracer held constant at 1 ppm below 500 m altitude and above having a lifetime of 6 h (T6h), and a second 20-days lifetime tracer held constant at 1 ppt at the surface (T20d).

Both models have an overall operator split timestep of 60 min, where large scale advection is treated for 60 min and then boundary layer mixing for 4×15 min. Constant T6h and T20d values (as described above) are set before every 15-min boundary layer mixing step, so that each mixing step will not experience a surface layer with almost no

Title Page

Abstract

Introduction

Conclusions

References

Tables

Figures



Back

Close

Full Screen / Esc

Printer-friendly Version

Interactive Discussion



T6h or T20d tracer available. This is mainly important for T20d, which is only set in the surface layer.

The T6h and T20d results for the same regions as in Hoyle et al. (2011), are shown in Fig. 8, where Oslo CTM3 in general has smaller mixing ratios for T6h than does the CTM2 (Up to 100 % difference at 200–100 hPa), and slightly smaller for T20d.

As described in Sect. 2.2.2, the CTM2 only uses updraft convective mass fluxes; convective downdrafts are not taken into account, and neither are detrainment rates into the up- or downdrafts. In Oslo CTM3, downdrafts and detrainment rates are also taken into account, and while downdrafts change the results negligibly (not shown), the use of detrainment rates explains most of the model differences in T6h above 550–300 hPa (dash-dotted lines in Fig. 8). At the surface there are little differences in T6h between CTM3 and CTM2, due to the constantly replenishing to 1 ppm below 500 m. Using the detrainment rates transports substantially less to high altitudes due to venting below, as explained in Sect. 2.2.2.

For T20d, the difference between CTM2 and CTM3 is smaller than for T6h, but skipping downdrafts and detrainments still shifts the CTM3 towards the CTM2 profiles above 700–550 hPa.

In general, the Oslo CTM3 transports up to ~10% less out of the lowermost model layers than CTM2, mainly in sub-tropical and mid-latitude regions. This may be due to small differences in the boundary layer schemes or in the different treatments of convection.

3.2.3 Vertical profiles – O₃ sondes

Vertical profiles of O₃, interpolated linearly to the location of selected sonde stations around the world, are put out hourly from the models. This allows reasonable temporal interpolations to sonde launch times, thereby giving a better basis for comparing modelled and observed profiles.

To evaluate the modelled O₃ in the troposphere, we compare the models to O₃ sonde measurements available from the World Ozone and Ultraviolet Radiation Data Centre

Title Page

Abstract

Introduction

Conclusions

References

Tables

Figures



Back

Close

Full Screen / Esc

Printer-friendly Version

Interactive Discussion



(WOUDC), and also from Southern Hemisphere ADditional OZonesondes (SHADOZ) (Thompson et al., 2003). As noted in Sect. 2.5, model emissions are for the year 2000, so we have chosen to use this year also for the sonde evaluation.

A few single sonde comparisons are shown in Fig. 9, and as the troposphere is of interest, the comparisons are carried out on linear axes. Observed profiles are shown in black, while C3_NIT is shown in red and C2_NIT in green. Both models are capable of reproducing the main structures of the single profiles, although small structures cannot be captured due to the vertical resolution of the models. It seems that CTM2 may capture folds better, however, shortening the transport time step does improve CTM3 tropopause folds (not shown).

As will be discussed in Sect. 3.3, CTM3 without nitrate aerosols produce slightly higher tropospheric O₃ than CTM2. However, excluding nitrate still reproduce sondes well (not shown).

We have also carried out sonde comparisons as monthly means, where model profiles only at measurement times have been used. Profiles for selected stations and months are shown in Fig. 10, where the profiles have been interpolated to a fixed pressure spacing, i.e. the 60-layer model spacing for a surface pressure of 1000 hPa, and from these the mean profiles were calculated.

Based on all sondes during each month, standard deviations are calculated and shown as horizontal bars. The hatched areas show the range of O₃ in the observations (backslashed black) and in the Oslo CTM3 profiles (slashed red).

In general the differences between CTM2 and CTM3 are small, however, for some of the locations and months, CTM2 reproduce measurements better, while CTM3 is best at other times and locations. Again, there are small differences between C3_NIT and C3, and between C2_NIT and C2, mainly in the upper troposphere and lowermost stratosphere (not shown).

Title Page

Abstract

Introduction

Conclusions

References

Tables

Figures



Back

Close

Full Screen / Esc

Printer-friendly Version

Interactive Discussion



3.3 Global diagnostics

Several global diagnostics are frequently used to evaluate atmospheric models, such as the average tropospheric OH concentration, the CH₄ lifetime, the O₃ burden and the mass flux of O₃ from the stratosphere into the troposphere. Here we present these and also the lifetime of N₂O.

The diagnostics are in general calculated within domains between the model surface and four different upper boundaries. These upper boundaries are our model tropopause (2.5 PVU), 200 hPa, the 150 ppb O₃ surface, and the model top (LTOP). The prior defines the tropopause at potential vorticity of 2.5 PVU (Holton et al. (1995), 1 PVU is 10⁻⁶ Km² kg⁻¹ s⁻¹), with an upper limit of 380 K potential temperature and a somewhat arbitrary lower limit of 5 km (only occurs occasionally).

3.3.1 OH concentration

OH is the main oxidizing species in the troposphere, driven by photolysis rates. It is usually referred to in context of CH₄ lifetime, which will be discussed in Sect. 3.3.2. Here we present average OH from the different year 2005 simulations carried out, calculated from monthly means of OH, air mass, pressure (p) and temperature (T). For 2005, the fraction of air below the CTM tropopause is 80.2 %, while below 200 hPa it is 79.7 %. The fraction below 150 ppb O₃, in general higher than 2.5 PVU, differs slightly for the different runs; 84.6 % for C3, 85.5 % for C3_NIT, 83.4 % for C2 and 83.5 % for C2_NIT.

Two averaging kernels are used to calculate OH average; first the OH concentration is weighted by air mass and by the loss rate to CH₄ ($\exp(-1775/T)$), and second it is weighted by air mass and a simplified loss rate of CO using pressure ($1 + 0.6p$). The values are presented in Table 4, showing small differences for the different model domains.

CTM3 has a larger OH than CTM2, partly due to fast-JX being photochemically more active than fast-J2 in CTM2, but also due to differences in wet scavenging. In

GMDD

5, 1561–1626, 2012

Oslo CTM3

O. A. Søvde et al.

Title Page

Abstract

Introduction

Conclusions

References

Tables

Figures

◀

▶

◀

▶

Back

Close

Full Screen / Esc

Printer-friendly Version

Interactive Discussion



Oslo CTM3

O. A. Søvde et al.

[Title Page](#)[Abstract](#)[Introduction](#)[Conclusions](#)[References](#)[Tables](#)[Figures](#)[Back](#)[Close](#)[Full Screen / Esc](#)[Printer-friendly Version](#)[Interactive Discussion](#)

simulation C3, the CH_4 loss weighted OH concentration is $\sim 1.55 \times 10^6 \text{ molec cm}^{-3}$, while in C2 it is $\sim 1.35 \times 10^6 \text{ molec cm}^{-3}$. C3_NIT and C2_NIT produce values of $\sim 1.33 \times 10^6 \text{ molec cm}^{-3}$ and $\sim 1.22 \times 10^6 \text{ molec cm}^{-3}$, respectively. For the OH average weighted against $(1 + 0.6p)$, the averages are about 10% smaller, but otherwise show the similar picture. Inclusion of sulfur and nitrate modules in CTM3 is important for OH, reducing it by 14–15%. For CTM2, however, this reduction is 10–11%.

For the NIT-simulations, some of the reduced OH may be due to sulfur chemistry removing some OH through oxidation processes. More important is the sequestering of NO_x in nitrate aerosols (Myhre et al., 2006), which with subsequent washout adds a removal process of atmospheric nitrogen and thus a source of OH. OH reduction due to the nitrate module is most pronounced in NH winter/spring, when the wind-driven production of sea salt is largest. As will be described in Sect. 3.4, the less efficient wet scavenging in CTM3 allows for more uptake of HNO_3 in nitrate aerosols, making the inclusion of nitrate aerosols more important in CTM3 than in CTM2. Because OH depends strongly on the amount of atmospheric NO_x and H_2O_2 , CTM3/CTM2 differences in wet scavenging of e.g. HNO_3 and H_2O_2 will be important. This will be addressed in Sect. 3.4.

The amount of CO in the atmosphere is important for OH levels, and while this cannot explain differences between CTM2 and CTM3, Lamarque et al. (2010) showed that the RETRO anthropogenic CO emissions are probably too low. Studies also show that atmospheric models tend to underestimate CO (Shindell et al., 2006; Isaksen et al., 2009), and other studies indicate that estimated CO emissions probably are too low (Pison et al., 2009; Kopacz et al., 2010). More recent emission inventories, with higher CO emissions, may contribute to lower the OH concentration, and will be studied with the Oslo CTM3 in the future.

Further, fast-JX allows for letting aerosols affect photochemistry through scattering and absorption, thereby possibly changing OH. Bian et al. (2003) reported that the effect of aerosols on photolysis would reduce OH by $\sim 8\%$. This will be investigated in the already-mentioned upcoming paper focusing on aerosols.

3.3.2 CH₄ and N₂O lifetimes

The lifetime of CH₄ is estimated to be 8.7 ± 1.3 yr (IPCC AR4, 2007), although recently, Prather et al. (2012) estimated the OH-lifetime of CH₄ to be 11.2 ± 1.3 yr and the total atmospheric lifetime to be 9.1 ± 0.9 yr. The main atmospheric sink of CH₄ is OH, predominantly in the troposphere. CH₄ is also lost to Cl and O¹(D), mainly in the stratosphere. However, Cl-chemistry also occur in the marine boundary layer. In CTM3 and CTM2, there is no halogen chemistry in the boundary layer, and loss to Cl and O¹(D) only occurs in the stratosphere. Another important sink is uptake by soil, however, due to the long lifetime of CH₄ models usually keep CH₄ at prescribed levels at the surface instead of including emissions and soil uptake. This is also done in CTM2 and CTM3.

Global mean CH₄ lifetimes for the year 2005 for all simulations are listed in Table 5, calculated from monthly accumulated CH₄ loss and the monthly mean CH₄ burden. Also listed are the ranges of monthly averages, and whereas OH on a monthly basis is highest during NH summer, CH₄ lifetime shows an opposite variation.

In-line with the larger OH in CTM3 compared to CTM2, its CH₄ lifetime is somewhat shorter than for CTM2. The change in OH due to inclusion of sulfur chemistry and nitrate aerosols clearly affect the lifetime; C3 produce a CH₄ lifetime of ~8 yr for 2005 for the tropospheric domains, while C3_NIT increase the lifetime to ~9.3 yr. The slight variation between the tropospheric domains are due to how much of the troposphere and stratosphere (i.e. chemistry) that is covered by each domain. The domain below 2.5 PVU only covers OH loss, while the domain below 200 hPa cuts off the uppermost tropical troposphere and includes high latitude stratosphere with loss due to Cl and O¹(D). The domain below 150 ppb O₃ extends above the 2.5 PVU domain and covers some stratospheric loss to Cl and O¹(D). Based on the whole model domain, the total lifetimes for C3_NIT and C2_NIT are 7.6 and 8.7 yr, respectively, giving a stratospheric lifetime of 150 yr. From the monthly mean concentrations and loss rates we also estimate that OH, Cl and O¹(D) contribute to the stratospheric lifetime by about 46 %, 25 % and 29 %, respectively.

GMDD

5, 1561–1626, 2012

Oslo CTM3

O. A. Søvde et al.

Title Page

Abstract

Introduction

Conclusions

References

Tables

Figures

◀

▶

◀

▶

Back

Close

Full Screen / Esc

Printer-friendly Version

Interactive Discussion



Oslo CTM3

O. A. Søvde et al.

[Title Page](#)[Abstract](#)[Introduction](#)[Conclusions](#)[References](#)[Tables](#)[Figures](#)[Back](#)[Close](#)[Full Screen / Esc](#)[Printer-friendly Version](#)[Interactive Discussion](#)

In other words, inclusion of sulfur and nitrate modules increases the CTM3 lifetime by about 1.2 yr. A tropospheric lifetime of ~ 9.3 yr is in better agreement with literature values (IPCC AR4, 2007). However, compared to Prather et al. (2012) our tropospheric OH-lifetime is slightly low, while the total atmospheric lifetime is within their range.

As mentioned in Sect. 3.3.1, inclusion of modelled aerosols in the photolysis calculations could reduce tropospheric OH by $\sim 8\%$ (Bian et al., 2003). From our monthly means of CH_4 , OH, Cl, $\text{O}(^1\text{D})$ and temperature we find that this could increase the OH-lifetime to ~ 10 yr and the total lifetime to ~ 9.4 yr, in better agreement with Prather et al. (2012).

However, it is worth mentioning that Prather et al. (2012) include surface emissions and loss and also marine boundary layer loss to chlorine, not treated in the CTM3. Using our OH-lifetime and stratospheric lifetime and following their method of calculations, we estimate that this could reduce our total lifetime by 7–10%.

Because of lower OH in CTM2, the CH_4 lifetime is longer; C2 produce a lifetime of ~ 9.2 yr, while C2.NIT increase it to ~ 10.2 yr. The increase due to inclusion of sulfate and nitrate is almost one year, somewhat less than for CTM3, as was found for OH reduction.

It should be noted, that within the whole model domain, the atmospheric amount of CH_4 in simulations C3 and C3.NIT are 4822 Tg and 4828 Tg, respectively, while C2 and C2.NIT produce 4830 Tg and 4831 Tg, respectively, about 2% lower than the estimated 4932 Tg (IPCC AR4, 2007).

Another important greenhouse gas is N_2O , which in general is inert in the troposphere, while having a small stratospheric loss. Hence, N_2O has a long lifetime, and in CTM3 we calculate it to be 144 yr, with a monthly average range of 133–155 yr. Because the photolysis code used in CTM2 (fast-J2) had smaller solar fluxes in the 200–230 nm region where N_2O and O_2 are photolyzed in most of the stratosphere, the N_2O lifetime in CTM2 is longer, 151 yr. Both of these lifetimes are probably too long because of stagnant vertical transport in the cycle 36r1 meteorology used in both calculations, somewhat evident in the underestimate of the CTM N_2O profiles (Fig. 6c).

3.3.3 O₃ burden

We have calculated the tropospheric burden of O₃ using the tropospheric domains defined in Sect. 3.3.2. The numbers are presented in Table 6, for the year 2005 and as the mean of years 1998 to 2005. Also the range of the monthly mean values for 2005 are listed.

The interannual variation is small, as are the differences between CTM3 and CTM2. Below the model tropopause the modelled burden in 2005 is 360 Tg for C3 and 302 Tg for C3_NIT, while the Oslo CTM2 produces 352 Tg for C2 and 326 Tg for C2_NIT. Similar values are found for the 1998–2005 averages.

Slightly lower O₃ burdens are calculated below 200 hPa, while below the 150 ppb O₃ surface, the modelled burdens are slightly higher, due to the vertical extent of the domains being slightly smaller and larger, respectively. However, the differences between C3 and C2 are smaller than between C3_NIT and C2_NIT.

Based on several model studies, Stevenson et al. (2006) presented a tropospheric burden range of 344 ± 39 Tg, however without a well-defined domain. Depending on which domain we use, the Oslo CTM3 can be placed within or just outside this range.

A halving of the operator split timestep (C3_30MIN) only changes the burden by ~2%, indicating that the tropospheric O₃ burden is not very sensitive to the transport time step. As noted in Sect. 3.3.2, the main differences between C2 and C3 are due to the new fast-JX photochemistry being somewhat more active, and differences in wet scavenging. Compared to C3, C3_NIT reduces the tropospheric O₃ burden by 50–60 Tg. This is about twice the change we see when including nitrate in CTM2, also showing that nitrate aerosols have become more important in CTM3.

3.3.4 Cross-tropopause O₃ flux

The stratosphere to troposphere exchange (STE) is the net flux from the stratosphere into the troposphere, and is estimated based on observations to be 540 ± 140 Tg(O₃)yr⁻¹ (Murphy and Fahey, 1994; Gettelman et al., 1997; IPCC AR4, 2007)

GMDD

5, 1561–1626, 2012

Oslo CTM3

O. A. Søvde et al.

Title Page

Abstract

Introduction

Conclusions

References

Tables

Figures

◀

▶

◀

▶

Back

Close

Full Screen / Esc

Printer-friendly Version

Interactive Discussion



Model studies suggest that STE range around 500 Tg (O₃) yr⁻¹ (McLinden et al., 2000; Olsen et al., 2001; Hsu et al., 2005; Stevenson et al., 2006).

In Oslo CTM3 the STE calculation follows Hsu et al. (2005). Due to technical challenges, this has not been possible in CTM2, and while Søvde et al. (2011a) presented CTM2 STE, their method is not comparable to the CTM3 treatment – hence we present only CTM3 in this study. During a certain time period in CTM3 (e.g. a month), STE of O₃ is calculated as a residual of column mass budgets between the model surface and a certain O₃ isopleth (Hsu et al., 2005). Below the given O₃ isopleth and for the given time period, this can be written

$$\left(\frac{dM}{dt}\right)_{\text{tot}} = \left(\frac{dM}{dt}\right)_{\text{chem}} - S + F_{s \rightarrow t} - F_{h,t \rightarrow t} \quad (7)$$

where $\left(\frac{dM}{dt}\right)_{\text{tot}}$ is the total change in O₃, $\left(\frac{dM}{dt}\right)_{\text{chem}}$ is the corresponding chemical tendency of O₃, S is sink processes such as dry deposition at the surface and wet scavenging, $F_{h,t \rightarrow t}$ is the horizontal flux of O₃ out of the column (troposphere to troposphere), and $F_{s \rightarrow t}$ is the STE to be inferred (both horizontal and vertical). Hence, the left-hand side of Eq. (7) is diagnosed as the change from the beginning to the end of the diagnosed time period, while the right-hand side terms are summed up for all time steps during the time period.

For the year 2005, using an O₃ isopleth of 120 ppb, Oslo CTM3 produce an annual STE of 315 Tg (O₃) yr⁻¹ for C3 and 275 Tg (O₃) yr⁻¹ for C3.NIT. The reduction in STE for C3.NIT is most probably due to a different 120 ppb isopleth. On a monthly basis, the STE is largest in NH summer, while smallest in NH winter. It can be argued that the STE should be calculated without the heterogeneous chemical reactions on polar stratospheric clouds, and a C3 test without PSCs increased the STE to 431 Tg (O₃) yr⁻¹ for 2005. The increase is partly due to changing the position of the 120 ppb isopleth.

With the C3_30MIN simulation, STE is slightly reduced to 295 Tg (O₃) yr⁻¹, due to a slightly changing O₃ isopleth, and less overshooting of the stratospheric jet.

[Title Page](#)[Abstract](#)[Introduction](#)[Conclusions](#)[References](#)[Tables](#)[Figures](#)[Back](#)[Close](#)[Full Screen / Esc](#)[Printer-friendly Version](#)[Interactive Discussion](#)

Oslo CTM3

O. A. Søvde et al.

[Title Page](#)[Abstract](#)[Introduction](#)[Conclusions](#)[References](#)[Tables](#)[Figures](#)[◀](#)[▶](#)[◀](#)[▶](#)[Back](#)[Close](#)[Full Screen / Esc](#)[Printer-friendly Version](#)[Interactive Discussion](#)

We have also carried out a 14 month simulation starting at 1 November 2004, using an older cycle of the ECMWF IFS meteorology (cycle 29). With this, the Oslo CTM3 produce a STE of 366 Tg (O_3) yr^{-1} . While this indicates that the old cycle may be more realistic, it should be noted that the N_2O blob is much less pronounced for cycle 29 meteorological data. Our comparison with MLS indicates that cycle 36r1 may have too stagnant vertical transport in the stratosphere, and UCI-CTM calculations of STE (Hsu and Prather, 2009) are considerably reduced when using cycle 36r1.

It may be that the chosen isopleth is not a representative surface for calculating STE. This should be studied further, using different isopleths. For 2005, we have used an alternative surface for calculating STE, namely the troposphere defined by the artificial e90-tracer (Prather et al., 2011), resulting in an annual STE of 279 Tg (O_3) yr^{-1} . In the future, other e90-surfaces will also be studied.

3.4 Wet scavenging

Wet removal of atmospheric HNO_3 and H_2O_2 are important for the NO_x and OH abundances. Less removal of H_2O_2 will increase tropospheric OH, and less removal of HNO_3 will increase atmospheric NO_x . Also important for the NO_x - O_3 cycle is scavenging of HO_2NO_2 , which is rapidly cycled to NO_x and back. HNO_3 can be recycled back to NO_x by either photodissociation or reaction with OH, but most of it is lost to the surface by wet or dry scavenging. In addition, NO_x will by itself change OH by shifting the HO_2 /OH balance.

Hence, if CTM3 wet scavenging is less efficient than for CTM2, the amount of OH and NO_x will be higher than in CTM2. Due to the complexity of the coupled system, it has not been possible to separate out the contributions to OH from increased NO_x due to the wet scavenging scheme from that due to the update to fast-JX.

It should be noted that a major difference from CTM2 to CTM3 scavenging is that CTM2 treats all large scale precipitation as liquid rain, while CTM3 separates it into ice and liquid precipitation. The only species removed by ice in CTM3 is HNO_3 , and even

that is reduced relative to liquid rain (CTM2). The convective scavenging scheme is the same in both, and treats all convective precipitation as convective rain.

To compare the wet scavenging in CTM3 to CTM2, we have carried out idealised 7-day simulations with only transport and wet removal of HNO_3 , H_2O_2 and HO_2NO_2 .

Tracer removals by large scale and convective precipitation are diagnosed hourly. We present results for 1–7 January 2005, but find similar results for other months. The idealised tracers are initialised from the C3_NIT simulation at 1 January 2005, and we find that CTM3 removes less in the upper troposphere, while removing slightly more in the lowermost tropical troposphere, similar to results in Neu and Prather (2012).

In total HNO_3 burden, CTM3 removes less HNO_3 than does CTM2; starting from a tropospheric burden of 1.43 Tg (HNO_3), CTM3 ends at 0.62 Tg (HNO_3) after 7 days, while CTM2 ends at 0.40 Tg (HNO_3). The higher HNO_3 in CTM3 is due to large scale precipitation being constrained by cloud fraction and hence less effective; the amount removed at each time step is about 30 to 40 % lower than for CTM2. Large changes in the initial scavenging rate occur because the initialized fields (C3_INIT) were inconsistent with the rapid large-scale scavenging in the upper troposphere by CTM2. By looking at the decay rates over the last few days of the experiment, when the HNO_3 distribution more closely matches each CTM's pattern of scavenging, we find that for CTM3 the effective tropospheric lifetime of HNO_3 is 6.9 days and for CTM2 it is 9.3 days, confirming the more rapid loss in CTM2.

The amount removed by convective scavenging is initially similar in CTM2 and CTM3, however, after a few time steps CTM3 removes more by convective scavenging than CTM2, compensating for the reduced large-scale scavenging. However, the fraction of tropospheric HNO_3 washed out by convective rain at each time step remains similar in CTM2 and CTM3, since the process is unchanged in the CTM update.

Less effective wet scavenging is also found for H_2O_2 in CTM3. The tropospheric H_2O_2 burden starts at 3.86 Tg, and after 7 days of only transport and wet scavenging CTM3 ends at 1.66 Tg, while CTM2 ends at 0.95 Tg. After 7 days this correspond to a tropospheric lifetime of 5.9 days for CTM2 and 11.4 days for CTM3. Initially, CTM2

[Title Page](#)

[Abstract](#)

[Introduction](#)

[Conclusions](#)

[References](#)

[Tables](#)

[Figures](#)



[Back](#)

[Close](#)

[Full Screen / Esc](#)

[Printer-friendly Version](#)

[Interactive Discussion](#)



Oslo CTM3

O. A. Søvde et al.

[Title Page](#)[Abstract](#)[Introduction](#)[Conclusions](#)[References](#)[Tables](#)[Figures](#)[Back](#)[Close](#)[Full Screen / Esc](#)[Printer-friendly Version](#)[Interactive Discussion](#)

removes about 4 times as much as CTM3 in large scale scavenging, which is a larger difference than for HNO_3 , because H_2O_2 is not removed by ice in CTM3 but is removed in CTM2. The fraction of the tropospheric burden removed by convective scavenging is smaller in CTM3, which was not the case for HNO_3 . While Neu and Prather (2012) found H_2O_2 uptake in ice to have a very small effect on O_3 , the differences from CTM2 to CTM3 may be large enough to re-examine this result.

HO_2NO_2 is scavenged only by convective rain in CTM2, which is considered a bug. This error was found after all simulations were finished, and due to computational limits we cannot repeat the full chemistry runs. CTM3 removes this species for both convective and large scale precipitation, but not by ice. With this lack of ice removal, we find that the amount removed by convective scavenging is similar in both models, but that CTM3 in total removes slightly more than CTM2 because of the included large scale scavenging. For HO_2NO_2 we find convective scavenging to be 2–3 times more important than large scale scavenging. If HO_2NO_2 should be found to be removed by ice precipitation, it would add an important sink for tropospheric NO_x thereby reducing O_3 (Neu and Prather, 2012).

Our chemistry simulations C2 and C3 show similar results; less HNO_3 is scavenged in CTM3, giving the latter a higher tropospheric burden of HNO_3 . The very different pattern of scavenging from CTM2 to CTM3 also contributes to this, by changing the relative distribution of HNO_3 throughout the troposphere. However, for the NIT simulations, the tropospheric burden in CTM3 is lower than for CTM2, even though CTM3 removes HNO_3 less efficiently by wet scavenging.

This somewhat counter-intuitive result comes about because of other HNO_3 loss processes, most importantly uptake in nitrate aerosols. The less efficient wet scavenging in CTM3 also applies for sea salt and nitrate aerosols, allowing more HNO_3 to be bound in nitrate particles, and is the reason why the inclusion of sulfur and nitrate modules is more important in CTM3 than in CTM2. Also important are differences in other loss processes such as photodissociation and the loss to OH. The smaller HNO_3 burden in CTM3 is not distributed evenly. In the tropics at altitudes below ~ 250 hPa, and in the

sub-tropics below ~ 700 hPa, CTM3 has up to twice as much HNO_3 , consistent with less efficient scavenging. Outside this region, the amount of HNO_3 is about half of that in CTM2, except in the upper stratosphere, where CTM3 again has somewhat higher HNO_3 .

The higher OH in CTM3 than in CTM2 is partly due to less removal of H_2O_2 ; the CTM3 burden of H_2O_2 is $\sim 12\%$ higher than for CTM2. Spatially, this difference comes from a decrease of $\sim 20\%$ in the tropical troposphere, but an increase of up to 400% in the upper troposphere due to lack of scavenging by ice. The more active photochemistry in fast-JX may dissociate more HNO_3 to NO_x , which again contribute to increasing OH and thereby to HNO_3 loss, but as already mentioned, it has not been possible to separate the effects of differences in scavenging and photochemistry.

Due to the erroneous lack of large scale HO_2NO_2 scavenging in CTM2, the CTM3 has a considerable lower amount of this tracer, especially in the upper troposphere and lower stratosphere.

3.5 Computational efficiency

Part of the motivation for updating the Oslo CTM2 was to make the transport faster, allowing long or complex chemistry simulations. To determine how much faster the Oslo CTM3 is than CTM2, and how well they scale to the number of CPUs used, we have carried out tests for the T42L60 dataset used. Both models are run for one month (January 2005), a month which was found to represent model transport times well, on an Intel Xeon with 32 X7560 2.27 GHz CPUs.

While the CTM2 transport is parallelized over number of tracers, CTM3 is parallelized over pre-defined horizontal blocks, except for the horizontal transport which is parallelized over model vertical layers. This allows the CTM3 to be run in parallel even for one tracer, and because most processes can be treated in horizontal blocks, matching the number of blocks to a multiple of the number of CPUs allows for a more efficient parallel code. This is an important improvement, making the CTM3 more flexible for using a higher number of CPUs.

Title Page

Abstract

Introduction

Conclusions

References

Tables

Figures



Back

Close

Full Screen / Esc

Printer-friendly Version

Interactive Discussion



Oslo CTM3

O. A. Søvde et al.

[Title Page](#)[Abstract](#)[Introduction](#)[Conclusions](#)[References](#)[Tables](#)[Figures](#)[Back](#)[Close](#)[Full Screen / Esc](#)[Printer-friendly Version](#)[Interactive Discussion](#)

Full chemistry simulations with CTM2 and CTM3 (C3) were timed for T42L60 resolution, and CTM3 was found to be about 40 % faster than CTM2. Pure transport tests reveal a somewhat better improvement, indicating that processes related to chemistry and diagnostics, which are now more realistic, take more time in Oslo CTM3 than in CTM2. The main contributors to this are the stratospheric microphysics which is treated with a time step of 15 min instead of one hour in CTM2, but to some extent also the fast-JX cloud overlap treatment, as described in Sect. 2.4.

Both models scale rather well with number of CPUs; a doubling of CPUs generally makes the runs ~40 % faster. However, the gain is reduced dramatically for the CTM2 full chemistry run when shifting from 16 to 32 CPUs due to the number of transported tracers badly matching the numbers of CPUs. CTM3 shows only a slightly lower improvement from 16 to 32 CPUs than from 8 to 16 CPUs. Increasing the number of CPUs also makes the fractional time spent on non-parallelized processes larger, which could also explain some of the inefficiency of increasing CPU numbers.

Pure transport simulations are also carried out in a higher horizontal resolution, namely T159L60 (1.125° × 1.125° degrees), showing a larger reduction (~60 %) in computing time from CTM2 to CTM3 than at T42L60 resolution. Hence, high resolution simulations have become more feasible with the Oslo CTM3.

4 Sensitivity studies

Some of the changes from CTM2 to CTM3 are quite substantial, and will contribute to changes in model results, either due to transport or through chemistry, even though the chemistry schemes are identical.

In order to document these changes, several 14-month sensitivity studies are carried out, listed in Table 2. In this Section we summarize the findings of halving the operator split time step and of using the more accurate V2 polar cap transport. Also, we document the changes due to updating the lightning NO_x vertical profiles from Pickering et al. (1998) to Ott et al. (2010).

4.1 Transport sensitivities

When halving the CTM3 operator split time step to 30 min (C3_30MIN), the computing time is increased by almost 100 %, because also chemistry is calculated with the same time step. In general there are small differences between C3 and C3_30MIN, except that the SH polar vortex edge seems to be better resolved in C3_30MIN, with a sharper gradient across the vortex edge. This corresponds well with what was seen for age of air. Total O₃ column values at the polar side of the SH vortex edge are reduced by up to 20 %, while on the mid-latitude side the column values are increased by up to 5 %. This can also be seen in the Northern Hemisphere, however to a smaller extent.

In the O₃ zonal monthly means (not shown), a pattern similar to the age of air results can be seen; halving the time step results in a more closed-off polar vortex in both hemispheres; the differences are mainly found at high latitudes between 300 hPa and 20 hPa. A halving of only the horizontal transport time step has also been tested, and found to produce somewhat sharper vortex gradients, although not to the same extent as for C3_30MIN. This indicates that vertical transport is important for a better resolved vortex edge.

Using the more accurate polar transport (C3_V2) increases the computing time by about 50 %. Hence, not all model time steps require shorter transport time steps than for C3. The changes from C3 are small, and generally confined to the polar cap. However, the shorter transport time steps produce a somewhat sharper gradient across the vortex edge than for C3.

Differences in C3_V2 compared to C3 become small when only the 1-D transport pipe time step is shortened, as this mainly increase computing time.

When V2 transport impose a shorter global time step the changes will essentially be similar to C3_30MIN, except that V2 does not change the chemical time step. However, if the global transport time step does not need to change, V2 may affect only the 1-D transport pipe, and thereby produce smaller differences between C3 and C3_V2. Again, this was also seen for the age of air studies.

GMDD

5, 1561–1626, 2012

Oslo CTM3

O. A. Søvde et al.

Title Page

Abstract

Introduction

Conclusions

References

Tables

Figures

◀

▶

◀

▶

Back

Close

Full Screen / Esc

Printer-friendly Version

Interactive Discussion



Studies involving stratospheric polar cap transport, e.g. Arctic and Antarctic O₃ loss studies, will clearly benefit from using V2-transport, perhaps also by using a 30 min overall time step. Other studies may benefit of the shorter computing time achieved by combining polar boxes and/or using a 60 min overall time step and find the performance acceptable.

4.2 L-NO_x vertical profiles

An Oslo CTM3 simulation using the old Pickering et al. (1998) lightning profiles is carried out, to show the effect of the new profiles available from Ott et al. (2010). This test is, however, not directly comparable to the Oslo CTM2, which use a slightly different horizontal lightning distribution.

The Pickering et al. (1998) distributions are referred to as “C”-shaped profiles, placing the largest fractions of the emissions close to the surface and close to the convective top. The Ott et al. (2010) profiles places the largest fractions somewhat lower than the convective top, and are referred to as backward-“C”-shaped profiles. In the Oslo CTM3 (C3), this changes the NO_x distribution, as seen in the annual zonal mean in Fig. 11a (as NO + NO₂), with the corresponding difference in O₃ in Fig. 11b.

Using the vertical profiles of Ott et al. (2010) produces up to 10% higher NO_x between 800 hPa and 400 hPa, compared to using Pickering et al. (1998). Above 200 hPa there is a decrease of up to ~20%, and at the surface decreases of up to ~30%. Correspondingly, the annual change in O₃ is slightly increased in some regions between 900 hPa and 500 hPa, and otherwise reduced by up to 3%, when using the new profiles. The decrease above 300 hPa is largest in winter. However, the changes are small, giving a negligibly lower tropospheric O₃ burden with the new profiles, and a 0.4% lower CH₄ lifetime. Selected O₃ sonde comparisons for the year 2005 show small differences (not shown).

Title Page

Abstract

Introduction

Conclusions

References

Tables

Figures



Back

Close

Full Screen / Esc

Printer-friendly Version

Interactive Discussion



5 Discussion and conclusions

We have presented the chemical transport model Oslo CTM3 and documented the changes from the earlier version Oslo CTM2. Thorough evaluation of the Oslo CTM3 against the Oslo CTM2 and against measurements have been carried out, showing that the new version is as good as, if not better than the old model.

Oslo CTM3 allows for stable, large time steps for advection, and this is essential in enabling more complex (e.g. fully coupled stratosphere-troposphere, gas-aerosol) CTM simulations. Nevertheless, the larger time steps result in larger errors, particularly near the jets where a curving flow may partly overshoot. When necessary, these errors can be reduced by using a shorter operator split time step (or advection time step) in the Oslo CTM3.

In general, Oslo CTM3 represents the stratosphere better than CTM2 due to the update to fast-JX. Total O₃ columns and burdens compare well with measurements and other model studies. In the troposphere there are some model differences due to differences in photochemical reaction rates and also due to different schemes for wet scavenging by rain. The CTM3 wet scavenging scheme is more physically based than the old version, although it removes slightly less of e.g. HNO₃ from the troposphere. CTM3 separates large scale scavenging by ice and rain, but the only species subject for ice scavenging is HNO₃. Because CTM2 assumes all precipitation to be rain, it generally scavenges more than CTM3 does. As a consequence, with only the tropospheric and stratospheric chemistry schemes included, NO_x is somewhat increased and OH is slightly high, giving a corresponding shorter CH₄ lifetime (8 yr). Including sulfur chemistry and nitrate aerosols improve this bias, increasing the CH₄ lifetime by ~16% to 9.3 yr. This increase is somewhat larger for CTM3 than for CTM2, making the inclusion of sulfate and nitrate modules more important in CTM3. The main reason is that the less efficient scavenging in CTM3 removes less sea salt aerosols, thereby allowing more HNO₃ to be bound in nitrate aerosols than in CTM2. As a consequence aerosol modules changes OH and hence the CH₄ lifetime more in CTM3 than in CTM2. It may

GMDD

5, 1561–1626, 2012

Oslo CTM3

O. A. Søvde et al.

Title Page

Abstract

Introduction

Conclusions

References

Tables

Figures



Back

Close

Full Screen / Esc

Printer-friendly Version

Interactive Discussion



also be that CO emissions used in this study are too low, and increasing the tropospheric CO may reduce the OH concentration and hence increase the CH₄ lifetime. This will be investigated in the future.

The new stratosphere to troposphere flux calculation through the 120 ppb O₃ surface yields a somewhat low value of 275–315 Tg(O₃) yr⁻¹ for the year 2005. Halving the transport time step reduces the STE slightly. Using an older cycle of ECMWF meteorological data, yields a higher flux more consistent with the semi-empirical STE fluxes of Murphy and Fahey (1994) and Olsen et al. (2001). This, and the model underestimate of N₂O compared with satellite observations, indicate that the ECMWF IFS cycle 36r1 has a degraded performance in the stratosphere with a too stagnant Brewer-Dobson circulation and slow upwelling in the tropics. It has not been possible to test the newer cycle 37. We have also shown that turning off PSC heterogeneous chemistry increase the calculated STE, partly due to changing of the 120 ppb surface. Further investigations should be carried out, using a set of isopleth values. Also other definitions of tropopause should be studied further, such as different threshold values for the e90 tracer.

Two polar cap transport treatments are available, and when studying polar cap transport care should be taken to use the most accurate method. Reducing the transport time step results in sharper polar vortex edges, and should be considered when studying processes close to or inside polar vortices.

It should be mentioned that the Oslo CTM3 also can be run without stratospheric chemistry, following a similar approach as in Skeie et al. (2011), using a model climatology for stratospheric O₃ and NO_x from a simulation with tropospheric and stratospheric chemistry. This would make the simulations faster, due to fewer transported species, and may be an option for studies of the lower to middle troposphere, where the importance of the stratosphere is small.

The Oslo CTM3 provides a large improvement of the Oslo CTM2, due to updated and more physically based parameterizations, and also due to the new structure, making the Oslo CTM3 up to 40% faster and better suited for parallelization. In addition,

Title Page

Abstract

Introduction

Conclusions

References

Tables

Figures



Back

Close

Full Screen / Esc

Printer-friendly Version

Interactive Discussion



the model source code is better structured, better commented and thereby easier to understand.

Acknowledgements. Thanks to the MLS team at the Jet Propulsion Laboratory, NASA, for providing satellite data, and also TOMS and OMI for providing O₃ columns.

5 Thanks to Meteorological Service of Canada, Alfred Wegener Institute – Ny Alesund, UK Meteorological Office, and Royal Meteorological Institute of Belgium for making O₃ sonde measurements available through the World Ozone and Ultraviolet Radiation Data Centre (WOUDC). Also thanks to SHADOZ for providing additional sonde measurements.

10 We also thank the European Centre for Medium-Range Weather Forecasts for providing meteorological data.

Thanks to L. T. Murray, GEOS-Chem developer at Harvard School of Engineering and Applied Sciences, for the vertical profile routine for lightning NO_x.

15 The work was of OAS was partly funded by the Norwegian Research Council, project number 171218 (Aerosol/gas-phase chemistry and microphysics in global models) and 208277 (Climate and health impacts of Short Lived Atmospheric Components), and also the EU project REACT4C, grant number ACP8-GA-2009-233772.

References

- 20 Allen, D., Pickering, K., Duncan, B., and Damon, M.: Impact of lightning NO emissions on North American photochemistry as determined using the Global Modeling Initiative (GMI) model, *J. Geophys. Res.*, 107, 4711, doi:10.1029/2010JD014062, 2010. 1574
- Allen, D. R., Douglass, A. R., Manney, G. L., Strahan, S. E., Krossschell, J. C., Trueblood, J. V., Nielsen, J. E., Pawson, S., and Zhu, Z.: Modeling the Frozen-In Anticyclone in the 2005 Arctic Summer Stratosphere, *Atmos. Chem. Phys.*, 11, 4557–4576, doi:10.5194/acp-11-4557-2011, 2011. 1580
- 25 Atkinson, R., Baulch, D. L., Cox, R. A., Crowley, J. N., Hampson, R. F., Hynes, R. G., Jenkin, M. E., Rossi, M. J., and Troe, J.: Evaluated kinetic and photochemical data for atmospheric chemistry: Volume I - gas phase reactions of O_x, HO_x, NO_x and SO_x species, *Atmos. Chem. Phys.*, 4, 1461–1738, doi:10.5194/acp-4-1461-2004, 2004. 1570

Title Page

Abstract

Introduction

Conclusions

References

Tables

Figures



Back

Close

Full Screen / Esc

Printer-friendly Version

Interactive Discussion



[Title Page](#)[Abstract](#)[Introduction](#)[Conclusions](#)[References](#)[Tables](#)[Figures](#)[◀](#)[▶](#)[◀](#)[▶](#)[Back](#)[Close](#)[Full Screen / Esc](#)[Printer-friendly Version](#)[Interactive Discussion](#)

- Balis, D., Isaksen, I. S. A., Zerefos, C., Zyrichidou, I., Eleftheratos, K., Tourpali, K., Bojkov, R., Rognerud, B., Stordal, F., Søvde, O. A., and Orsolini, Y.: Observed and modelled record ozone decline over the Arctic during winter/spring 2011, *Geophys. Res. Lett.*, 38, L23801, doi:10.1029/2011GL049259, 2011. 1578
- 5 Berglen, T. F., Berntsen, T. K., Isaksen, I. S. A., and Sundet, J. K.: A global model of the coupled sulfur/oxidant chemistry in the troposphere: the sulfur cycle, *J. Geophys. Res.*, 109, D19310, doi:10.1029/2003JD003948, 2004. 1562, 1563, 1565, 1569, 1575
- Berntsen, T. and Isaksen, I. S. A.: A global 3-D chemical transport model for the troposphere, 1, Model description and CO and Ozone results, *J. Geophys. Res.*, 102, 21239–21280, doi:10.1029/97JD01140, 1997. 1565
- 10 Berntsen, T. K. and Isaksen, I. S. A.: Effects of lightning and convection on changes in upper tropospheric ozone due to NO_x emissions from aircraft, *Tellus B*, 51, 766–788, doi:10.1034/j.1600-0889.1999.t01-3-00003.x, 1999. 1573
- Bian, H., Prather, M. J., and Takemura, T.: Tropospheric aerosol impacts on trace gas budgets through photolysis, *J. Geophys. Res.*, 108, 4242, doi:10.1029/2002JD002743, 2003. 1585, 1587
- 15 Bian, H. S. and Prather, M. J.: Fast-J2: accurate simulation of stratospheric photolysis in global chemical models, *J. Atmos. Chem.*, 41, 281–296, doi:10.1023/A:1014980619462, 2002. 1570
- 20 Christian, H. J., Blakeslee, R. J., Boccippio, D. J., Boeck, W. L., Buechler, D. E., Driscoll, K. T., Goodman, S. J., Hall, J. M., Mach, D. A., and Stewart, M. F.: Global frequency and distribution of lightning as observed by the Optical Transient Dector (OTD), in: *Proceedings of the 11th International Conference on Atmospheric Electricity*, Guntersville, Alabama, 726–729, 1999a. 1573
- 25 Christian, H. J., Blakeslee, R. J., Goodman, S. J., Mach, D. A., Stewart, M. F., Buechler, D. E., Koshak, W. J., Hall, J. M., Boeck, W. L., Driscoll, K. T., and Boccippio, D. J.: The lightning imaging sensor, in: *Proceedings of the 11th International Conference on Atmospheric Electricity*, Guntersville, Alabama, 746–749, 1999b. 1573
- 30 Dalsøren, S. B., Endresen, Ø., Isaksen, I. S. A., Gravir, G., and Sørsgård, E.: Environmental impacts of the expected increase in sea transportation, with a particular focus on oil and gas scenarios for Norway and Northwest Russia, *J. Geophys. Res.*, 112, D02310, doi:10.1029/2005JD006927, 2007. 1562

[Title Page](#)[Abstract](#)[Introduction](#)[Conclusions](#)[References](#)[Tables](#)[Figures](#)[Back](#)[Close](#)[Full Screen / Esc](#)[Printer-friendly Version](#)[Interactive Discussion](#)

- Dalsøren, S. B., Eide, M. S., Myhre, G., Endresen, Ø., Isaksen, I. S. A., and Fuglestvedt, J. S.: Impacts of the large increase in international ship traffic 2000–2007 on tropospheric ozone and methane, *Environ. Sci. Technol.*, 44, 2482–2489, doi:10.1021/es902628e, 2010. 1563
- Froidevaux, L., Jiang, Y. B., Lambert, A., Livesey, N. J., Read, W. G., Waters, J. W., Browell, E. V., Hair, J. W., Avery, M. A., McGee, T. J., Twigg, L. W., Sunnicht, G. K., Jucks, K. W., Margitan, J. J., Sen, B., Stachnik, R. A., Toon, G. C., Bernath, P. F., Boone, C. D., Walker, K. A., Filipiak, M. J., Harwood, R. S., Fuller, R. A., Manney, G. L., Schwartz, M. J., Daffer, W. H., Drouin, B. J., Cofield, R. E., Cuddy, D. T., Jarnot, R. F., Knosp, B. W., Perun, V. S., Snyder, W. V., Stek, P. C., Thurstans, R. P., and Wagner, P. A.: Validation of aura microwave limb sounder stratospheric ozone measurements, *J. Geophys. Res.*, 113, D15S20, doi:10.1029/2007JD008771, 2008. 1579
- Gauss, M.: Impact of aircraft emissions and ozone changes in the 21st century: 3-D model studies, Ph.D. thesis, University of Oslo, Department of Geophysics, Section of Meteorology and Oceanography, PB. 1022 Blindern, 0315 Oslo, Norway, ISSN 1501-7710, No. 304, 2003. 1565
- Gauss, M., Isaksen, I. S. A., Wong, S., and Wang, W. C.: Impact of H₂O emissions from cryoplanes and kerosene aircraft on the atmosphere, *J. Geophys. Res.*, 108, 4304, doi:10.1029/2002JD002623, 2003. 1562
- Gauss, M., Isaksen, I. S. A., Lee, D. S., and Søvde, O. A.: Impact of aircraft NO_x emissions on the atmosphere – tradeoffs to reduce the impact, *Atmos. Chem. Phys.*, 6, 1529–1548, doi:10.5194/acp-6-1529-2006, 2006. 1562
- Gettelman, A., Holton, J. R., and Rosenlof, K. H.: Mass fluxes of O₃, CH₄, N₂O, and CF₂Cl₂ in the lower stratosphere calculated from observational data, *J. Geophys. Res.*, 102, 19149–19159, doi:10.1029/97JD01014, 1997. 1588
- Grini, A., Myhre, G., Sundet, J. K., and Isaksen, I. S. A.: Modeling the annual cycle of sea salt in the global 3-D model Oslo CTM-2, *J. Climate*, 15, 1717–1730, doi:10.1175/1520-0442(2002)015<1717:MTACOS>2.0.CO;2, 2002. 1563, 1565, 1575
- Grini, A., Myhre, G., Zender, C., and Isaksen, I. S. A.: Model simulation of dust sources and transport in the global atmosphere. Effects of soil erodibility and wind speed variability, *J. Geophys. Res.*, 110, D02205, doi:10.1029/2004JD005037, 2005. 1563
- Hall, T. M. and Prather, M. J.: Simulations of the trend and annual cycle in stratospheric CO₂, *J. Geophys. Res.*, 98, 10573–10581, doi:10.1029/93JD00325, 1993. 1563

[Title Page](#)[Abstract](#)[Introduction](#)[Conclusions](#)[References](#)[Tables](#)[Figures](#)[Back](#)[Close](#)[Full Screen / Esc](#)[Printer-friendly Version](#)[Interactive Discussion](#)

- Hall, T. M. and Prather, M. J.: Seasonal evolutions of N_2O , O_3 , and CO_2 : Three-dimensional simulations of stratospheric correlations, *J. Geophys. Res.*, 100, 16699–16720, doi:10.1029/94JD03300, 1995. 1563
- Hall, T. M., Waugh, D. W., Boering, K. A., and Plumb, R. A.: Evaluation of transport in stratospheric models, *J. Geophys. Res.*, 104, 18815–18839, doi:10.1029/1999JD900226, 1999. 1576
- Hodnebrog, Ø., Berntsen, T. K., Dessens, O., Gauss, M., Grewe, V., Isaksen, I. S. A., Koffi, B., Myhre, G., Oliví, D., Prather, M. J., Pyle, J. A., Stordal, F., Szopa, S., Tang, Q., van Velthoven, P., Williams, J. E., and Ødemark, K.: Future impact of non-land based traffic emissions on atmospheric ozone and OH – an optimistic scenario and a possible mitigation strategy, *Atmos. Chem. Phys.*, 11, 11293–11317, doi:10.5194/acp-11-11293-2011, 2011. 1563
- Holton, J. R., Haynes, P. H., McIntyre, M. E., Douglass, A. R., Rood, R. B., and Pfister, L.: Stratosphere-troposphere exchange, *Rev. Geophys.*, 33, 403–439, doi:10.1029/95RG02097, 1995. 1584
- Holtstlag, A. A. M., DeBrujin, E. I. F., and Pan, H.-L.: A high resolution air mass transformation model for short-range weather forecasting, *Mon. Weather Rev.*, 118, 1561–1575, doi:10.1175/1520-0493(1990)118<1561:AHRAMT>2.0.CO;2, 1990. 1566
- Hoor, P., Borken-Kleefeld, J., Caro, D., Dessens, O., Endresen, O., Gauss, M., Grewe, V., Hauglustaine, D., Isaksen, I. S. A., Jöckel, P., Lelieveld, J., Myhre, G., Meijer, E., Olivie, D., Prather, M., Schnadt Poberaj, C., Shine, K. P., Staehelin, J., Tang, Q., van Aardenne, J., van Velthoven, P., and Sausen, R.: The impact of traffic emissions on atmospheric ozone and OH: results from QUANTIFY, *Atmos. Chem. Phys.*, 9, 3113–3136, doi:10.5194/acp-9-3113-2009, 2009. 1563
- Hoyle, C. R., Marécal, V., Russo, M. R., Allen, G., Arteta, J., Chemel, C., Chipperfield, M. P., D'Amato, F., Dessens, O., Feng, W., Hamilton, J. F., Harris, N. R. P., Hosking, J. S., Lewis, A. C., Morgenstern, O., Peter, T., Pyle, J. A., Reddmann, T., Richards, N. A. D., Telford, P. J., Tian, W., Viciani, S., Volz-Thomas, A., Wild, O., Yang, X., and Zeng, G.: Representation of tropical deep convection in atmospheric models – Part 2: Tracer transport, *Atmos. Chem. Phys.*, 11, 8103–8131, doi:10.5194/acp-11-8103-2011, 2011. 1581, 1582, 1623
- Hsu, J. and Prather, M. J.: Stratospheric variability and tropospheric ozone, *J. Geophys. Res.*, 114, D06102, doi:10.1029/2008JD010942, 2009. 1570, 1590

Hsu, J., Prather, M. J., and Wild, O.: Diagnosing the stratosphere-to-troposphere flux of ozone in a chemistry transport model, *J. Geophys. Res.*, 110, D19305, doi:10.1029/2005JD006045, 2005. 1589

IPCC AR4: Climate Change 2007: The Physical Science Basis. Contribution of Working Group I to the Fourth Assessment Report of the Intergovernmental Panel on Climate Change, Cambridge University Press, Cambridge, UK and New York, NY, USA, 996 pp., 2007. 1586, 1587, 1588

Isaksen, I. S. A., Zerefos, C., Kourtidis, K., Meleti, C., Dalsøren, S. B., Sundet, J. K., Grini, A., Zanis, P., and Balis, D.: Tropospheric ozone changes at unpolluted and semipolluted regions induced by stratospheric ozone changes, *J. Geophys. Res.*, 110, D02302, doi:10.1029/2004JD004618, 2005. 1562

Isaksen, I. S. A., Granier, C., Myhre, G., Berntsen, T., Dalsøren, S., Gauss, M., Klimont, Z., Benestad, R., Bousquet, P., Collins, W., Cox, T., Eyring, V., Fowler, D., Fuzzi, S., Jöckel, P., Laj, P., Lohmann, U., Maione, M., Monks, P., Prevot, A., Raes, F., Richter, A., Rognerud, B., Schulz, M., Shindell, D., Stevenson, D., Storelvmo, T., Wang, W.-C., van Weele, M., Wild, M., and Wuebbles, D.: Atmospheric composition change: climate-chemistry interactions, *Atmos. Environ.*, 43, 5138–5192, doi:10.1016/j.atmosenv.2009.08.003, 2009. 1585

Jackman, C. H., Marsh, D. R., Vitt, F. M., Garcia, R. R., Fleming, E. L., Labow, G. J., Randall, C. E., López-Puertas, M., Funke, B., von Clarmann, T., and Stiller, G. P.: Short- and medium-term atmospheric constituent effects of very large solar proton events, *Atmos. Chem. Phys.*, 8, 765–785, doi:10.5194/acp-8-765-2008, 2008. 1579

Jonson, J. E., Sundet, J. K., and Tarrason, L.: Model calculations of present and future levels of ozone and ozone precursors with a global and a regional model, *Atmos. Environ.*, 35, 525–537, doi:10.1016/S1352-2310(00)00314-9, 2001. 1563

Kärcher, B. and Voigt, C.: Formation of nitric acid/water ice particles in cirrus clouds, *Geophys. Res. Lett.*, 33, L08806, doi:10.1029/2006GL025927, 2006. 1569

Kopacz, M., Jacob, D. J., Fisher, J. A., Logan, J. A., Zhang, L., Megretskaia, I. A., Yantosca, R. M., Singh, K., Henze, D. K., Burrows, J. P., Buchwitz, M., Khlystova, I., McMillan, W. W., Gille, J. C., Edwards, D. P., Eldering, A., Thouret, V., and Nedelec, P.: Global estimates of CO sources with high resolution by adjoint inversion of multiple satellite datasets (MOPITT, AIRS, SCIAMACHY, TES), *Atmos. Chem. Phys.*, 10, 855–876, doi:10.5194/acp-10-855-2010, 2010. 1585

GMDD

5, 1561–1626, 2012

Oslo CTM3

O. A. Søvde et al.

Title Page

Abstract

Introduction

Conclusions

References

Tables

Figures

◀

▶

◀

▶

Back

Close

Full Screen / Esc

Printer-friendly Version

Interactive Discussion



Oslo CTM3

O. A. Søvde et al.

[Title Page](#)[Abstract](#)[Introduction](#)[Conclusions](#)[References](#)[Tables](#)[Figures](#)[Back](#)[Close](#)[Full Screen / Esc](#)[Printer-friendly Version](#)[Interactive Discussion](#)

- Lamarque, J.-F., Bond, T. C., Eyring, V., Granier, C., Heil, A., Klimont, Z., Lee, D., Lioussé, C., Mieville, A., Owen, B., Schultz, M. G., Shindell, D., Smith, S. J., Stehfest, E., Van Aardenne, J., Cooper, O. R., Kainuma, M., Mahowald, N., McConnell, J. R., Naik, V., Riahi, K., and van Vuuren, D. P.: Historical (1850–2000) gridded anthropogenic and biomass burning emissions of reactive gases and aerosols: methodology and application, *Atmos. Chem. Phys.*, 10, 7017–7039, doi:10.5194/acp-10-7017-2010, 2010. 1572, 1585
- Lambert, A., Read, W. G., Livesey, N. J., Santee, M. L., Manney, G. L., Froidevaux, L., Wu, D. L., Schwartz, M. J., Pumphrey, H. C., Jimenez, C., Nedoluha, G. E., Cofield, R. E., Cuddy, D. T., Daffer, W. H., Drouin, B. J., Fuller, R. A., Jarnot, R. F., Knosp, B. W., Pickett, H. M., Perrin, V. S., Snyder, W. V., Stek, P. C., Thurstans, R. P., Wagner, P. A., Waters, J. W., Jucks, K. W., Toon, G. C., Stachnik, R. A., Bernath, P. F., Boone, C. D., Walker, K. A., Urbani, J., Murtagh, D., Elkins, J., and Atlas, E.: Validation of the Aura Microwave Limb Sounder stratospheric water vapor and nitrous oxide measurements, *J. Geophys. Res.*, 112, D24S36, doi:10.1029/2007JD008724, 2007. 1579
- Livesey, N. J., Read, W. G., Froidevaux, L., Lambert, A., Manney, G. L., Pumphrey, H. C., Santee, M. L., Schwartz, M. J., Wang, S., Cofield, R. E., Cuddy, D. T., Fuller, R. A., Jarnot, R. F., Jiang, J. H., Knosp, B. W., Stek, P. C., Wagner, P. A., and Wu, D. L.: Earth Observing System (EOS) Aura Microwave Limb Sounder (MLS) Version 3.3 Level 2 data quality and description document, Tech. Rep. JPL D-33509, Jet Propulsion Laboratory, California Institute of Technology, Pasadena, California, 91109–8099, available at: <http://mls.jpl.nasa.gov> (last access: 18 January 2011), 2011. 1579
- Manney, G. L., Santee, M. L., Froidevaux, L., Hoppel, K., Livesey, N. J., and Waters, J. W.: EOS MLS observations of ozone loss in the 2004–2005 Arctic winter, *Geophys. Res. Lett.*, 33, L04802, doi:10.1029/2005GL024494, 2006. 1567, 1580
- McLinden, C. A., Olsen, S. C., Hannegan, B. J., Wild, O., Prather, M. J., and Sundet, J.: Stratosphere ozone in 3-D models: a simple chemistry and the cross-tropopause flux, *J. Geophys. Res.*, 105, 14653–14666, doi:10.1029/2000JD900124, 2000. 1589
- Murphy, D. M. and Fahey, D. W.: An estimate of the flux of stratospheric reactive nitrogen and ozone into the troposphere, *J. Geophys. Res.*, 99, 5325–5332, doi:10.1029/93JD03558, 1994. 1588, 1598
- Murray, L. T., Jacob, D. J., Logan, J. A., Hudman, R. C. and Koshak, W. J.: Optimized regional and interannual variability of lightning in a global chemical transport model constrained by LIS/OTD satellite data, *J. Geophys. Res.*, submitted, 2012. 1574

Oslo CTM3

O. A. Søvde et al.

[Title Page](#)[Abstract](#)[Introduction](#)[Conclusions](#)[References](#)[Tables](#)[Figures](#)[Back](#)[Close](#)[Full Screen / Esc](#)[Printer-friendly Version](#)[Interactive Discussion](#)

- Myhre, G., Grini, A., and Metzger, S.: Modelling of nitrate and ammonium-containing aerosols in presence of sea salt, *Atmos. Chem. Phys.*, 6, 4809–4821, doi:10.5194/acp-6-4809-2006, 2006. 1563, 1565, 1575, 1585
- 5 Myhre, G., Shine, K., Rädcl, G., Gauss, M., Isaksen, I., Tang, Q., Prather, M., Williams, J., van Velthoven, P., Dessens, O., Koffi, B., Szopa, S., Hoor, P., Grewe, V., Borken-Kleefeld, J., Berntsen, T., and Fuglestvedt, J.: Radiative forcing due to changes in ozone and methane caused by the transport sector, *Atmos. Environ.*, 45, 387–394, doi:10.1016/j.atmosenv.2010.10.001, 2011. 1563
- 10 Neu, J. L. and Prather, M. J.: Toward a more physical representation of precipitation scavenging in global chemistry models: cloud overlap and ice physics and their impact on tropospheric ozone, *Atmos. Chem. Phys.*, 12, 3289–3310, doi:10.5194/acp-12-3289-2012, 2012. 1563, 1569, 1591, 1592
- 15 Neu, J. L., Prather, M. J., and Penner, J. E.: Global atmospheric chemistry: integrating over fractional cloud cover, *J. Geophys. Res.*, 112, D11306, doi:10.1029/2006JD008007, 2007. 1563, 1570, 1571, 1572, 1610
- Olsen, S. C., McLinden, C. A., and Prather, M. J.: Stratospheric N₂O-NO_y system: testing uncertainties in a three-dimensional framework, *J. Geophys. Res.*, 106, 28771–28784, doi:10.1029/2001JD000559, 2001. 1589, 1598
- 20 Ott, L. E., Pickering, K. E., Stenchikov, G. L., Allen, D. J., DeCaria, A. J., Ridley, B., Lin, R.-F., Lang, S., and Tao, W.-K.: Production of lightning NO_x and its vertical distribution calculated from three-dimensional cloud-scale chemical transport model simulations, *J. Geophys. Res.*, 115, D04301, doi:10.1029/2009JD011880, 2010. 1574, 1575, 1594, 1596, 1626
- Owen, B., Lee, D. S., and Lim, L.: Flying into the future: aviation emissions scenarios to 2050, *Environ. Sci. Technol.*, 44, 2255–2260, doi:10.1021/es902530z, 2010. 1572
- 25 Pickering, K. E., Wang, Y. S., Tao, W. K., Price, C., and Muller, J. F.: Vertical distributions of lightning NO_x for use in regional and global chemical transport models, *J. Geophys. Res.*, 103, 31203–31216, doi:10.1029/98JD02651, 1998. 1575, 1594, 1596, 1626
- Pison, I., Bousquet, P., Chevallier, F., Szopa, S., and Hauglustaine, D.: Multi-species inversion of CH₄, CO and H₂ emissions from surface measurements, *Atmos. Chem. Phys.*, 9, 5281–5297, doi:10.5194/acp-9-5281-2009, 2009. 1585
- 30 Prather, M., McElroy, M., Wofsy, S., Russell, G., and Rind, D.: Chemistry of the global troposphere: fluorocarbons as tracers of air motion, *J. Geophys. Res.*, 92, 6579–6613, doi:10.1029/JD092iD06p06579, 1987. 1563

[Title Page](#)[Abstract](#)[Introduction](#)[Conclusions](#)[References](#)[Tables](#)[Figures](#)[Back](#)[Close](#)[Full Screen / Esc](#)[Printer-friendly Version](#)[Interactive Discussion](#)

- Prather, M. J.: Fast-JX version 6.5, available at: <http://www.ess.uci.edu/~prather/fastJX.html> (last access: 1 September 2009), 2009. 1570
- Prather, M. J.: Numerical advection by conservation of second-order moments, *J. Geophys. Res.*, 91, 6671–6681, doi:10.1029/JD091iD06p06671, 1986. 1565, 1566
- 5 Prather, M. J., Zhu, X., Strahan, S. E., Steenrod, S. D., and Rodriguez, J. M.: Quantifying errors in trace species transport modeling, *P. Natl. Acad. Sci. USA*, 105, 19617–19621, doi:10.1073/pnas.0806541106, 2008. 1563, 1566, 1575, 1576, 1577
- Prather, M. J., Zhu, X., Tang, Q., Hsu, J., and Neu, J. L.: An atmospheric chemist in search of the tropopause, *J. Geophys. Res.*, 116, D04304, doi:10.1029/2010JD014939, 2011. 1563, 1577, 1590
- 10 Prather, M. J., Holmes, C. D., and Hsu, J.: Reactive greenhouse gas scenarios: systematic exploration of uncertainties and the role of atmospheric chemistry, *Geophys. Res. Lett.*, 39, L09803, doi:10.1029/2012GL051440, 2012. 1586, 1587
- Price, C. and Rind, D.: A simple lightning parameterization for calculating global lightning distributions, *J. Geophys. Res.*, 97, 9919–9933, doi:10.1029/92JD00719, 1992. 1573, 1574, 1575
- 15 Randall, C. E., Harvey, V. L., Singleton, C. S., Bernath, P. F., Boone, C. D., and Kozyra, J. U.: Enhanced NO_x in 2006 linked to strong upper stratospheric Arctic vortex, *Geophys. Res. Lett.*, 33, L18811, doi:10.1029/2006GL027160, 2006. 1579
- 20 Randall, C. E., Harvey, V. L., Siskind, D., France, J., Bernath, P., Boone, C. D., and Walker, K.: NO_x descent in the Arctic middle atmosphere in early 2009, *Geophys. Res. Lett.*, 36, L18811, doi:10.1029/2009GL039706, 2009. 1579
- RETRO emissions: REanalysis of the TROpospheric chemical composition over the past 40 yr, available at: <http://retro.enes.org/> (last access: 11 June 2007), 2006. 1572
- 25 Sander, S. P., Finlayson-Pitts, B. J., Friedl, R. R., Golden, D. M., Huie, R. E., Keller-Rudek, H., Kolb, C. E., Kurylo, M. J., Molina, M. J., Moortgat, G. K., Orkin, V. L., Ravishankara, A. R., and Wine, P. H.: Chemical Kinetics and Photochemical Data for Use in Atmospheric Studies, Evaluation No. 15, Tech. Rep. 06-2, Jet Propulsion Laboratory, Pasadena, California Institute of Technology, available at: <http://jpldataeval.jpl.nasa.gov/> (last access: 6 September 2006), 2006. 1570
- 30 Sander, S. P., Abbatt, J., Barker, J. R., Burkholder, J. B., Friedl, R. R., Golden, D. M., Huie, R. E., Kolb, C. E., Kurylo, M. J., Moortgat, G. K., Orkin, V. L., and Wine, P. H.: Chemical Kinetics and Photochemical Data for Use in Atmospheric Studies, Evaluation No. 17, Tech. Rep.

Oslo CTM3

O. A. Søvde et al.

Title Page

Abstract

Introduction

Conclusions

References

Tables

Figures



Back

Close

Full Screen / Esc

Printer-friendly Version

Interactive Discussion



10-06, Jet Propulsion Laboratory, Pasadena, California Institute of Technology, available at: <http://jpldataeval.jpl.nasa.gov/> (last access: 10 June 2011), 2011. 1570

Santee, M. L., Lambert, A., Read, W. G., Livesey, N. J., Cofield, R. E., Cuddy, D. T., Daffer, W. H., Drouin, B. J., Froidevaux, L., Fuller, R. A., Jarnot, R. F., Knosp, B. W., Manney, G. L., Perun, V. S., Snyder, W. V., Stek, P. C., Thurstans, R. P., Wagner, P. A., Waters, J. W., Muscari, G., de Zafra, R. L., Dibb, J. E., Fahey, D. W., Popp, P. J., Marcy, T. P., Jucks, K. W., Toon, G. C., Stachnik, R. A., Bernath, P. F., Boone, C. D., Walker, K. A., Urban, J., and Murtagh, D.: Validation of the Aura Microwave Limb Sounder HNO₃ measurements, *J. Geophys. Res.*, 112, D24S40, doi:10.1029/2007JD008721, 2007. 1579

Semane, N., Teitelbaum, H., and Basdevant, C.: A very deep ozone minihole in the Northern Hemisphere stratosphere at mid-latitudes during the winter of 2000, *Tellus*, 54, 382–389, doi:10.1034/j.1600-0870.2002.01380.x, 2002. 1578

Semeniuk, K., Fomichev, V. I., McConnell, J. C., Fu, C., Melo, S. M. L., and Usoskin, I. G.: Middle atmosphere response to the solar cycle in irradiance and ionizing particle precipitation, *Atmos. Chem. Phys.*, 11, 5045–5077, doi:10.5194/acp-11-5045-2011, 2011. 1579

Shindell, D. T., Faluvegi, G., Stevenson, D. S., Krol, M. C., Emmons, L. K., Lamarque, J.-F., Pétron, G., Dentener, F. J., Ellingsen, K., Schultz, M. G., Wild, O., Amann, M., Atherton, C. S., Bergmann, D. J., Bey, I., Butler, T., Cofala, J., Collins, W. J., Derwent, R. G., Doherty, R. M., Drevet, J., Eskes, H. J., Fiore, A. M., Gauss, M., Hauglustaine, D. A., Horowitz, L. W., Isaksen, I. S. A., Lawrence, M. G., Montanaro, V., Müller, J.-F., Pitari, G., Prather, M. J., Pyle, J. A., Rast, S., Rodriguez, J. M., Sanderson, M. G., Savage, N. H., Strahan, S. E., Sudo, K., Szopa, S., Unger, N., van Noije, T. P. C., and Zeng, G.: Multimodel simulations of carbon monoxide: comparison with observations and projected near-future changes, *J. Geophys. Res.*, 111, D19306, doi:10.1029/2006JD007100, 2006. 1585

Skeie, R. B., Berntsen, T. K., Myhre, G., Tanaka, K., Kvalevåg, M. M., and Hoyle, C. R.: Anthropogenic radiative forcing time series from pre-industrial times until 2010, *Atmos. Chem. Phys.*, 11, 11827–11857, doi:10.5194/acp-11-11827-2011, 2011. 1565, 1598

Solberg, S., Coddeville, P., De Backer, H., C. Forster, Ø. H., Orsolini, Y., Uhse, K., Isaksen, I. S. A., and Søvde, A.: European surface ozone in the extreme summer 2003, *J. Geophys. Res.*, 113, D07307, doi:10.1029/2007JD009098, 2008. 1562

Søvde, O. A., Gauss, M., Smyshlyaev, S. P., and Isaksen, I. S. A.: Evaluation of the chemical transport model Oslo CTM2 with focus on Arctic winter ozone depletion, *J. Geophys. Res.*, 113, D09304, doi:10.1029/2007jd009240, 2008. 1563, 1565, 1578

Oslo CTM3

O. A. Søvde et al.

[Title Page](#)[Abstract](#)[Introduction](#)[Conclusions](#)[References](#)[Tables](#)[Figures](#)[Back](#)[Close](#)[Full Screen / Esc](#)[Printer-friendly Version](#)[Interactive Discussion](#)

- Søvde, O. A., Hoyle, C. R., Myhre, G., and Isaksen, I. S. A.: The HNO_3 forming branch of the $\text{HO}_2 + \text{NO}$ reaction: pre-industrial-to-present trends in atmospheric species and radiative forcings, *Atmos. Chem. Phys.*, 11, 8929–8943, doi:10.5194/acp-11-8929-2011, 2011a. 1563, 1589
- 5 Søvde, O. A., Orsolini, Y. J., Jackson, D. R., Stordal, F., Isaksen, I. S. A., and Rognerud, B.: Estimation of Arctic O_3 loss during winter 2006/2007 using data assimilation and comparison with a chemical transport model, *Q. J. Roy. Meteorol. Soc.*, 137, 118–128, doi:10.1002/qj.740, 2011b. 1565, 1578
- Stevenson, D. S., Dentener, F. J., Schultz, M. G., Ellingsen, K., van Noije, T. P. C., Wild, O., Zeng, G., Amann, M., Atherton, C. S., Bell, N., Bergmann, D. J., Bey, I., Butler, T., Co-fala, J., Collins, W. J., Derwent, R. G., Doherty, R. M., Drevet, J., Eskes, H. J., Fiore, A. M., Gauss, M., Hauglustaine, D. A., Horowitz, L. W., Isaksen, I. S. A., Krol, M. C., Lamarque, J.-F., Lawrence, M. G., Montanaro, V., Müller, J.-F., Pitari, G., Prather, M. J., Pyle, J. A., Rast, S., Rodriguez, J. M., Sanderson, M. G., Savage, N. H., Shindell, D. T., Strahan, S. E., Sudo, K., and Szopa, S.: Multimodel ensemble simulations of present-day and near-future tropospheric ozone, *J. Geophys. Res.*, 111, D08301, doi:10.1029/2005JD006338, 2006. 1588, 1589
- 15 Stordal, F., Isaksen, I. S. A., and Horntvedt, K.: A diabatic circulation two-dimensional model with photochemistry: Simulations of ozone and long-lived tracers with surface sources, *J. Geophys. Res.*, 90, 5757–5776, doi:10.1029/JD090iD03p05757, 1985. 1565
- 20 Sundet, J. K.: Model Studies with a 3-D Global CTM using ECMWF data, Ph.D. thesis, University of Oslo, Department of Geophysics, Section of Meteorology and Oceanography, PB. 1022 Blindern, 0315 Oslo, Norway, 1997. 1563
- Thompson, A. M., Witte, J., McPeters, R., Oltmans, S., Schmidlin, F., Logan, J., M. Fujiwara, Kirchhoff, V., Posny, F., Coetzee, G., Hoegger, B., Kawakami, S., Ogawa, T., Johnson, B., Vömel, H., and Labow, G.: Southern Hemisphere Additional Ozonesondes (SHADOZ) 1998–2000 tropical ozone climatology 1. Comparison with Total Ozone Mapping Spectrometer (TOMS) and ground-based measurements, *J. Geophys. Res.*, 108, 8238, doi:10.1029/2001JD000967, 2003. 1583
- 25 Tiedtke, M.: A comprehensive mass flux scheme for cumulus parameterisation on large scale models, *Mon. Weather Rev.*, 117, 1779–1800, doi:10.1175/1520-0493(1989)117<1779:ACMFSF>2.0.CO;2, 1989. 1565
- 30 Verronen, P. T., Funke, B., López-Puertas, M., Stiller, G. P., von Clarmann, T., Glatthor, N., Enell, C.-F., Turunen, E., and Tamminen, J.: About the increase of HNO_3 in the stratopause

[Title Page](#)[Abstract](#)[Introduction](#)[Conclusions](#)[References](#)[Tables](#)[Figures](#)[Back](#)[Close](#)[Full Screen / Esc](#)[Printer-friendly Version](#)[Interactive Discussion](#)

region during the Halloween 2003 solar proton event, *Geophys. Res. Lett.*, 35, L20809, doi:10.1029/2008GL035312, 2008. 1579

Verronen, P. T., Santee, M. L., Manney, G. L., Lehmann, R., Salmi, S.-M., and Seppala, A.: Nitric acid enhancements in the mesosphere during the January 2005 and December 2006 solar proton events, *J. Geophys. Res.*, 116, D17301, doi:10.1029/2011JD016075, 2011. 1579

Wesely, M. L.: Parameterization of surface resistances to gaseous dry deposition in regional-scale numerical models, *Atmos. Environ.*, 23, 1293–1304, 1989. 1569

Wild, O., Sundet, J. K., Prather, M. J., Isaksen, I. S. A., Akimoto, H., Browell, E. V., and Oltmans, S. J.: Chemical transport model ozone simulations for spring 2001 over the Western Pacific: comparisons with TRACE-P lidar, ozonesondes, and total ozone mapping spectrometer columns, *J. Geophys. Res.*, 108, 8826, doi:10.1029/2002JD003283, 2003. 1562

Williams, E.: Large-scale charge separation in thunderclouds, *J. Geophys. Res.*, 90, 6013–6025, doi:10.1029/JD090iD04p06013, 1985. 1573

Williamson, D. L., Drake, J. B., Hack, J. J., Jakob, R., and Swarztrauber, P. N.: A standard test set for numerical approximations to the shallow water equations in spherical geometry, *J. Comput. Phys.*, 102, 211–224, doi:10.1016/S0021-9991(05)80016-6, 1992. 1567

Oslo CTM3

O. A. Søvde et al.

[Title Page](#)[Abstract](#)[Introduction](#)[Conclusions](#)[References](#)[Tables](#)[Figures](#)[Back](#)[Close](#)[Full Screen / Esc](#)[Printer-friendly Version](#)[Interactive Discussion](#)**Table 1.** The main improvements documented in this work.

- | | |
|---|---|
| a | A new advection core that greatly speeds up the model, enabling more complex chemistry or very-high resolution (T319) chemistry simulations. |
| b | New, modernized lightning NO _x parameterizations that reflect current satellite observations and recent campaigns. |
| c | New scavenging scheme that includes liquid and ice water and partially overlapping clouds. |
| d | New fast-JX combined with the cloud overlap scheme (Neu et al., 2007) with an additional speed up from Neu's quadrature to a randomly selected cloud profile selected hourly based on the cloud fractions and overlaps from the ECMWF forecast data. |
| e | New convection treatment using ECMWF-diagnosed entrainment and detrainment, along with combining the convection and large-scale vertical advection to save time and reduce noise in redundant vertical transport where the inferred convective subsidence nearly cancels the large scale convergence. |
| f | Speed-up can increase transport errors near the jet streams, but this can be fixed by cutting the time step (and losing part of the speed-up). |

Oslo CTM3

O. A. Søvde et al.

Table 2. Description of the full transport-chemistry simulations in this study. The notation C2 and C3 represents CTM2 and CTM3, respectively. Lightning parameterizations are described in Sect. 2.6.

Simulation	Start	End	Lightning (see text)	Detrainment rates used?	Chemistry Trop/Strat/Nit	Operator split time step
C3	1 Jan 1997	31 Dec 2005	OTT	Yes	Y/Y/N	60 min
C3_NIT	1 Jan 1997	31 Dec 2005	OTT	Yes	Y/Y/Y	60 min
C2	1 Jan 1997	31 Dec 2005	C2PIC	no	Y/Y/N	60 min
C2_NIT	1 Jan 1997	31 Dec 2005	C2PIC	no	Y/Y/Y	60 min
C3_30MIN	1 Nov 2004	31 Dec 2005	OTT	Yes	Y/Y/N	30 min
C3_V2	1 Nov 2004	31 Dec 2005	OTT	Yes	Y/Y/N	60 min
C3_PIC	1 Nov 2004	31 Dec 2005	PIC	Yes	Y/Y/N	60 min

[Title Page](#)[Abstract](#)[Introduction](#)[Conclusions](#)[References](#)[Tables](#)[Figures](#)[Back](#)[Close](#)[Full Screen / Esc](#)[Printer-friendly Version](#)[Interactive Discussion](#)

Table 4. Annual average of OH in the atmosphere, calculated from monthly means of OH, air mass, temperature (T) and pressure (p , in bars), for the air mass below the model PVU-based tropopause height, air mass below 200 hPa, air mass below the modelled 150 ppb O_3 surface, and the air mass in the whole model domain (up to top level LTOP). The average OH concentration is weighted by air mass and by (a) the loss rate of CH_4 ($\exp(-1775/T)$) and (b) the approximate loss rate of CO ($1 + 0.6p$). All numbers are for the year 2005, and the ranges of monthly means are given in parentheses.

a. $[OH]$ ($10^6 \text{ molec cm}^{-3}$) weighted by air mass and $\exp(-1775/T)$.
Diagnosed between surface and selected upper boundaries.

Sim.	2.5 PVU	200 hPa	150 ppb O_3	LTOP
C3	1.55 (1.47–1.70)	1.54 (1.46–1.70)	1.54 (1.46–1.70)	1.55 (1.47–1.69)
C3_NIT	1.34 (1.24–1.52)	1.33 (1.23–1.51)	1.33 (1.22–1.51)	1.34 (1.24–1.51)
C2	1.35 (1.27–1.49)	1.34 (1.26–1.48)	1.35 (1.26–1.48)	1.35 (1.28–1.48)
C2_NIT	1.22 (1.11–1.36)	1.21 (1.11–1.36)	1.21 (1.11–1.36)	1.22 (1.13–1.37)

b. $[OH]$ ($10^6 \text{ molec cm}^{-3}$) weighted by air mass and $(1 + 0.6p)$.
Diagnosed between surface and selected upper boundaries.

Sim.	2.5 PVU	200 hPa	150 ppb O_3	LTOP
C3	1.40 (1.33–1.54)	1.39 (1.32–1.53)	1.39 (1.32–1.53)	1.37 (1.30–1.50)
C3_NIT	1.20 (1.08–1.36)	1.18 (1.08–1.35)	1.18 (1.08–1.34)	1.16 (1.06–1.32)
C2	1.21 (1.13–1.34)	1.20 (1.12–1.32)	1.21 (1.13–1.33)	1.18 (1.11–1.31)
C2_NIT	1.09 (0.99–1.23)	1.07 (0.97–1.21)	1.08 (0.98–1.22)	1.06 (0.97–1.20)

[Title Page](#)
[Abstract](#)
[Introduction](#)
[Conclusions](#)
[References](#)
[Tables](#)
[Figures](#)
[Back](#)
[Close](#)
[Full Screen / Esc](#)
[Printer-friendly Version](#)
[Interactive Discussion](#)


[Title Page](#)[Abstract](#)[Introduction](#)[Conclusions](#)[References](#)[Tables](#)[Figures](#)[◀](#)[▶](#)[◀](#)[▶](#)[Back](#)[Close](#)[Full Screen / Esc](#)[Printer-friendly Version](#)[Interactive Discussion](#)

Table 5. Annual average lifetimes of CH₄ (τ_{CH_4}), diagnosed as the total CH₄ burden (surface to model top) divided by the loss of CH₄ within the four diagnosed domains: Below the model PVU-based tropopause height, below 200 hPa surface, below the modelled 150 ppb O₃ surface, and the whole model domain (up to top level LTOP). All numbers are for the year 2005, and the ranges of monthly means are given in parentheses.

τ_{CH_4} (yr). Diagnosed between surface and selected upper boundaries.				
Sim.	2.5 PVU	200 hPa	150 ppb O ₃	LTOP
C3	7.98 (6.96–8.62)	8.03 (7.02–8.67)	7.94 (6.94–8.56)	7.55 (6.64–8.11)
C3_NIT	9.28 (7.82–10.32)	9.35 (7.88–10.41)	9.25 (7.80–10.27)	8.74 (7.45–9.64)
C2	9.18 (7.98–10.06)	9.26 (8.06–10.15)	9.14 (7.95–10.01)	8.64 (7.59–9.39)
C2_NIT	10.20 (8.68–11.43)	10.31 (8.77–11.55)	10.16 (8.65–11.37)	9.54 (8.22–10.58)

[Title Page](#)[Abstract](#)[Introduction](#)[Conclusions](#)[References](#)[Tables](#)[Figures](#)[Back](#)[Close](#)[Full Screen / Esc](#)[Printer-friendly Version](#)[Interactive Discussion](#)**Table 6.** Modelled annual average O₃ burden [Tg (O₃)] for different definitions of tropospheric domains.

Simulation	Diagnosed between surface and a selection of upper boundaries.					
	2.5 PVU		200 hPa		150 ppb O ₃	
	2005	1998–2005	2005	1998–2005	2005	1998–2005
C3	360 (340–386)	360	356 (342–374)	357	391 (373–415)	390
C3_NIT	302 (282–332)	302	299 (282–321)	300	338 (318–364)	337
C2	352 (336–376)	354	344 (331–355)	347	372 (358–389)	373
C2_NIT	326 (309–352)	328	317 (303–331)	321	346 (332–366)	347

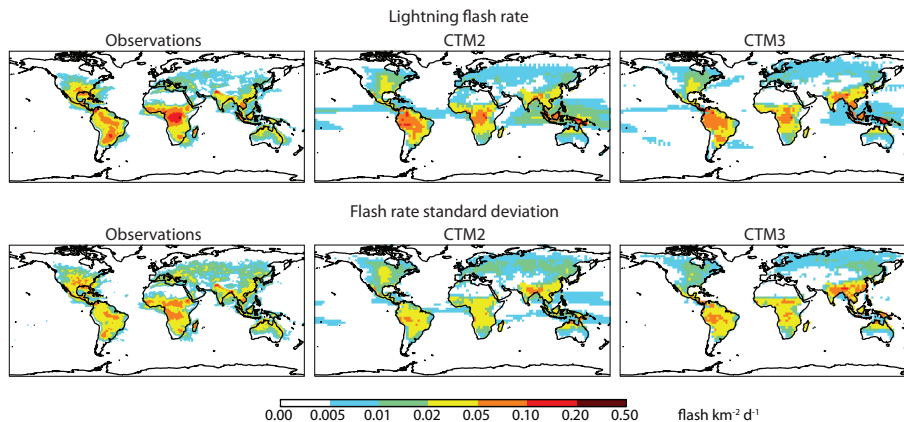


Fig. 1. Climatology of lightning flashes in observations and models. Annual mean flash rate (top) and standard deviation of monthly flash rates (bottom). Observation panels show OTD-LIS during 1995–2005. Model panels show Oslo CTM2 and Oslo CTM3 for 1999–2009.

[Title Page](#)[Abstract](#)[Introduction](#)[Conclusions](#)[References](#)[Tables](#)[Figures](#)[Back](#)[Close](#)[Full Screen / Esc](#)[Printer-friendly Version](#)[Interactive Discussion](#)

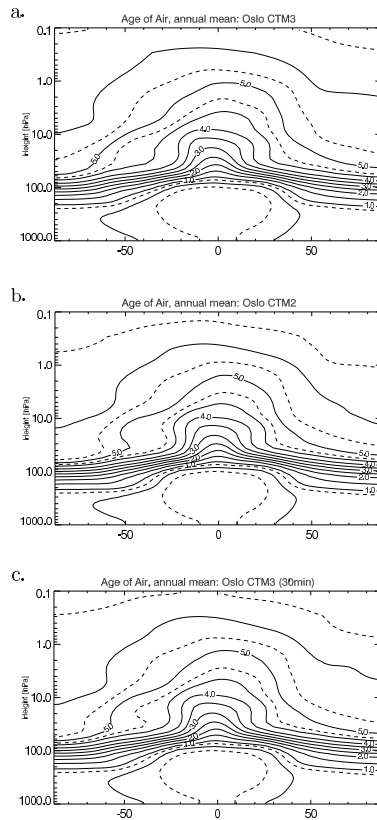


Fig. 2. Annual zonal mean age of air based on a tropical source tracer increasing linearly with time, after 20 yr of transport, resolution T42L60. **(a)** CTM3, **(b)** CTM2 and **(c)** CTM3 with 30 min operator split time step.

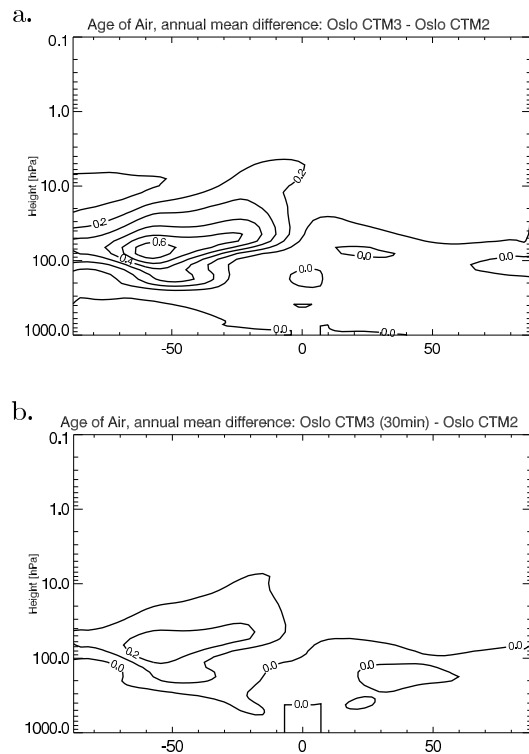


Fig. 3. Difference in annual zonal mean age of air between C3_AGE and C2_AGE (a) and C3_AGE_30MIN and C2_AGE (b).

[Title Page](#)[Abstract](#)[Introduction](#)[Conclusions](#)[References](#)[Tables](#)[Figures](#)[Back](#)[Close](#)[Full Screen / Esc](#)[Printer-friendly Version](#)[Interactive Discussion](#)

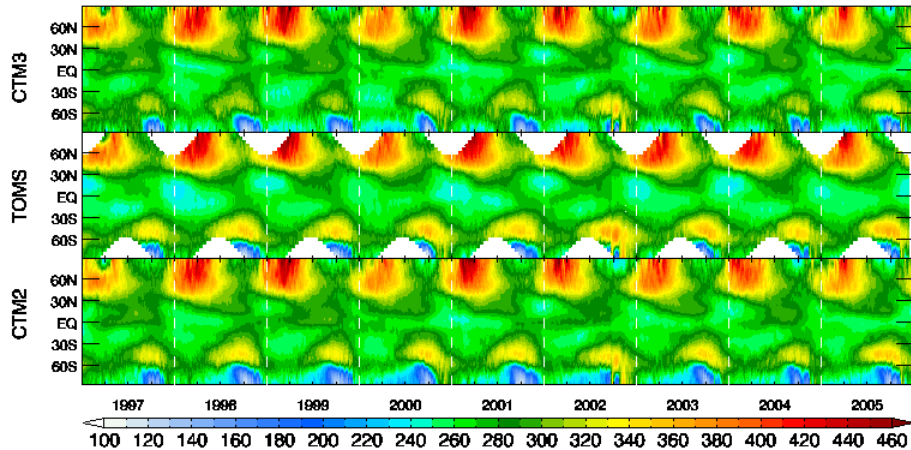


Fig. 4. Daily zonal mean total O₃ column (Dobson Units) for C3_NIT (top), TOMS (middle) and C2_NIT (bottom), from 1997 through 2005.

[Title Page](#)

[Abstract](#)

[Introduction](#)

[Conclusions](#)

[References](#)

[Tables](#)

[Figures](#)



[Back](#)

[Close](#)

[Full Screen / Esc](#)

[Printer-friendly Version](#)

[Interactive Discussion](#)



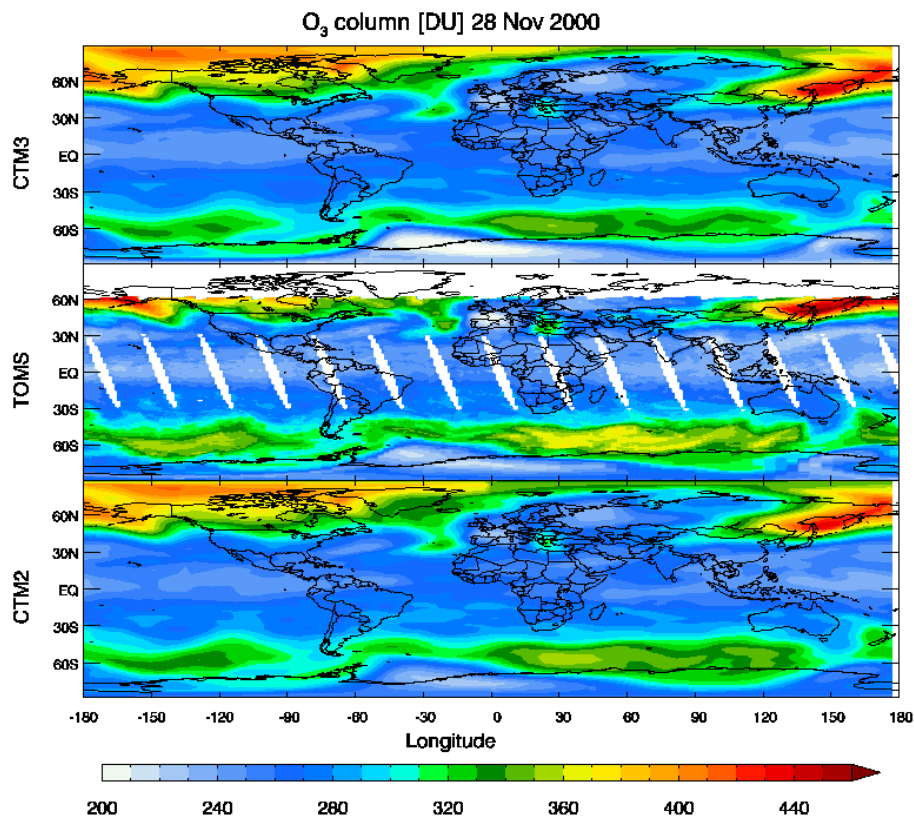


Fig. 5. Daily mean total O₃ column for C3_NIT (top), TOMS (middle) and C2_NIT (bottom), 28 Nov 2000.

Title Page

Abstract

Introduction

Conclusions

References

Tables

Figures



Back

Close

Full Screen / Esc

Printer-friendly Version

Interactive Discussion



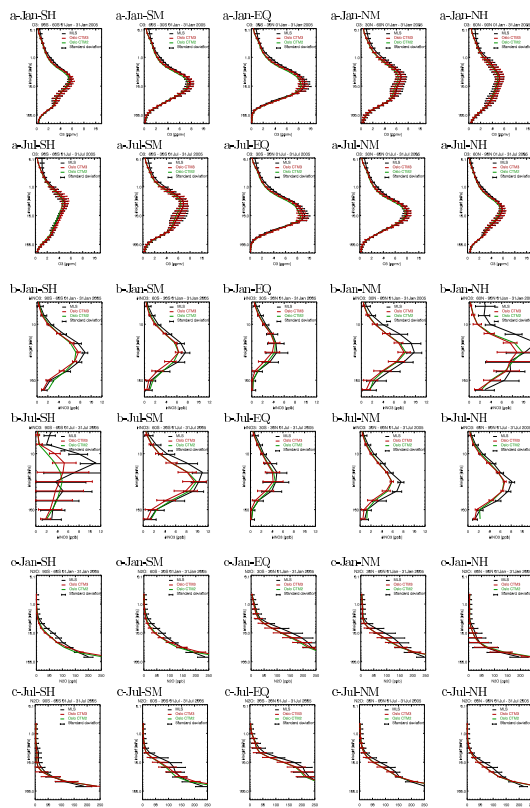


Fig. 6. Comparison of O₃ (label starts with “a”), HNO₃ (“b”) and N₂O (“c”) from CTM3 (C3_NIT), CTM2 (C2_NIT) and MLS, as vertical profiles of zonal monthly means covering the latitude bands 90° S–60° S (southern high, end-label “SH”), 60° S–30° S (southern mid-lat, “SM”), 30° S–30° N (“EQ”), 30° N–60° N (“NM”) and 60° N–90° N (“NH”) for January 2005 and July 2005. Model profiles are processed with the MLS averaging kernel and a-priori profiles.

[Title Page](#)
[Abstract](#)
[Introduction](#)
[Conclusions](#)
[References](#)
[Tables](#)
[Figures](#)

[Back](#)
[Close](#)
[Full Screen / Esc](#)
[Printer-friendly Version](#)
[Interactive Discussion](#)

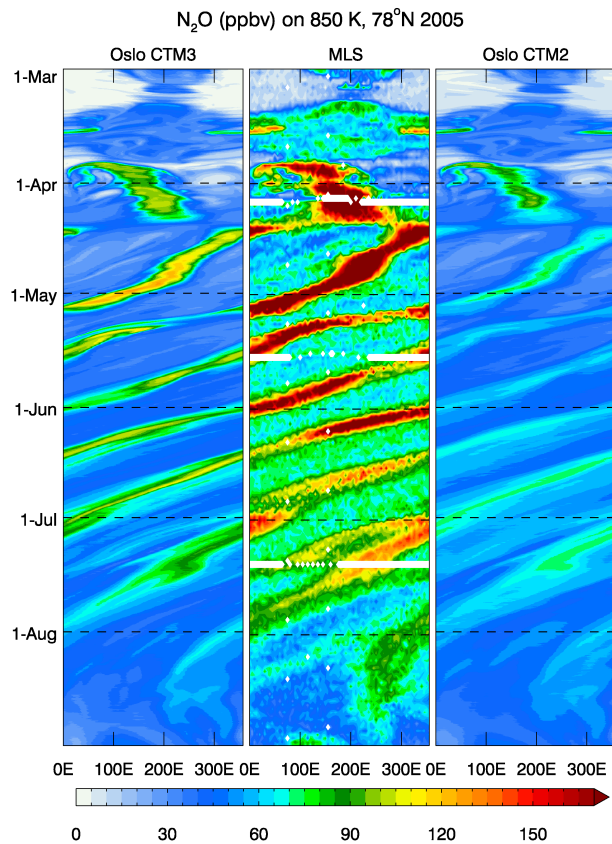



Fig. 7. Hovmöller plot of N₂O at 850 K and 78° N, as modelled by Oslo CTM3 (left), measured by MLS (middle) and modelled by Oslo CTM2 (right).

[Title Page](#)

[Abstract](#)

[Introduction](#)

[Conclusions](#)

[References](#)

[Tables](#)

[Figures](#)



[Back](#)

[Close](#)

[Full Screen / Esc](#)

[Printer-friendly Version](#)

[Interactive Discussion](#)



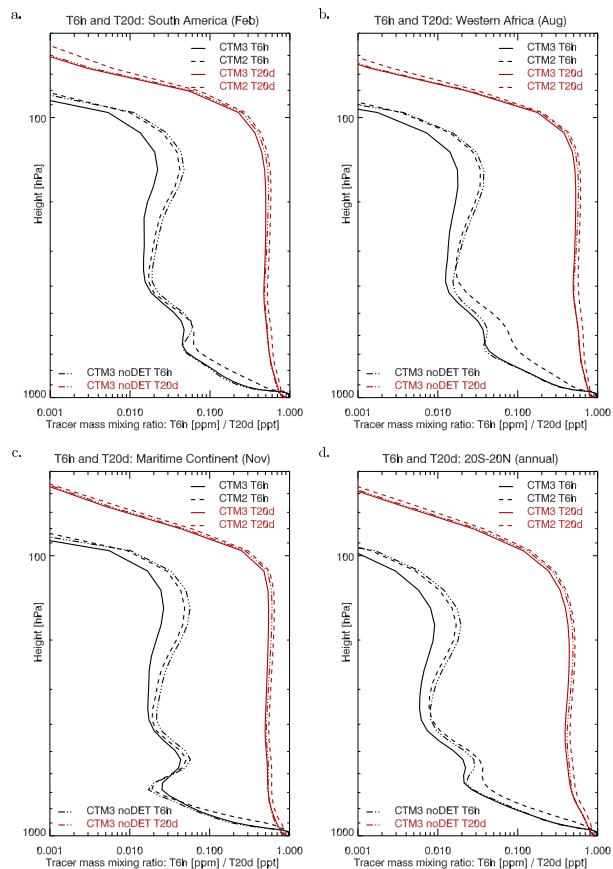


Fig. 8. T6h (ppm) and T20d (ppt) tracer as described in text and by Hoyle et al. (2011): selected monthly means for regions and annual mean for 20° S–20° N.

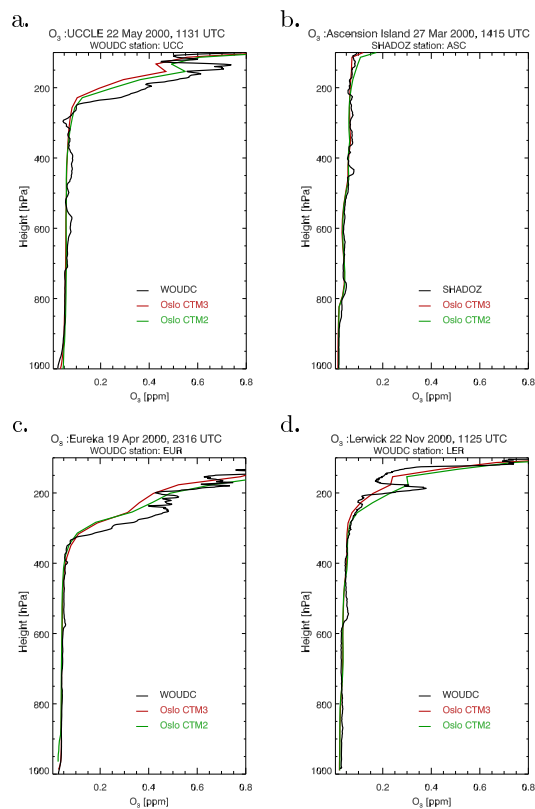


Fig. 9. Modelled and measured O_3 vertical profiles at selected sonde stations and launch times.

[Title Page](#)
[Abstract](#)
[Introduction](#)
[Conclusions](#)
[References](#)
[Tables](#)
[Figures](#)
[Back](#)
[Close](#)
[Full Screen / Esc](#)
[Printer-friendly Version](#)
[Interactive Discussion](#)

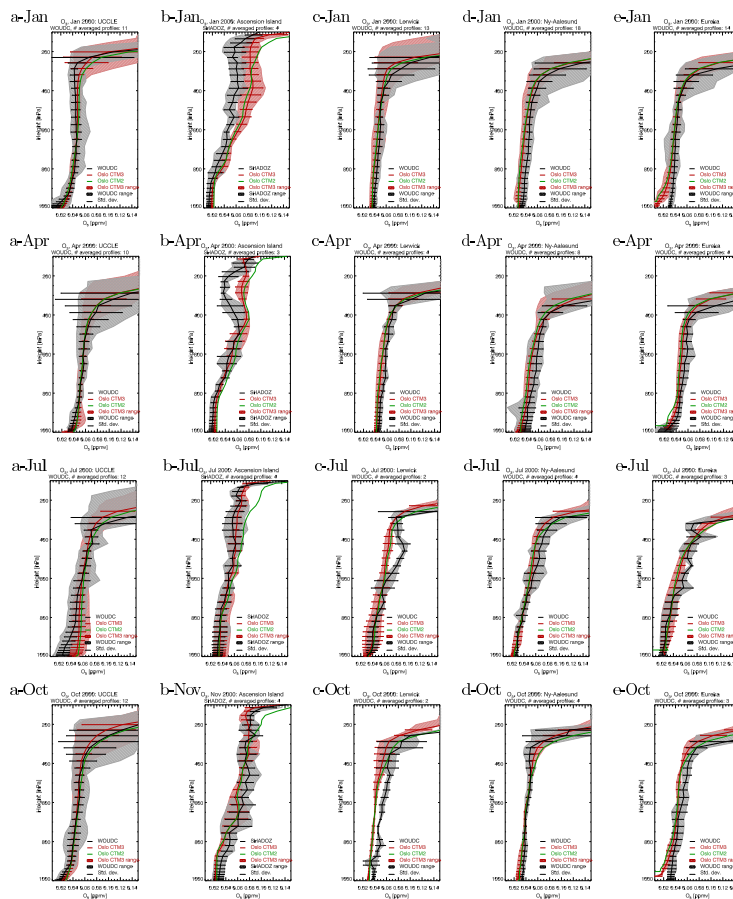



Fig. 10. Modelled (C3_NIT and C2_NIT) and measured monthly mean vertical profiles of O_3 at selected sonde stations (a–e). Different months for each station are shown in columns.

[Title Page](#)
[Abstract](#)
[Introduction](#)
[Conclusions](#)
[References](#)
[Tables](#)
[Figures](#)

[Back](#)
[Close](#)
[Full Screen / Esc](#)
[Printer-friendly Version](#)
[Interactive Discussion](#)

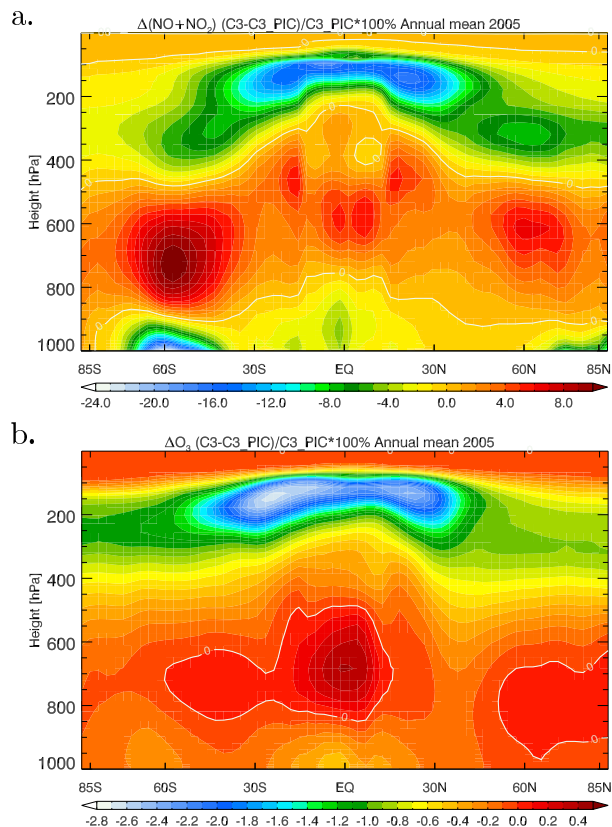



Fig. 11. Annual zonal mean percent difference in $\text{NO} + \text{NO}_2$ and O_3 between two runs using lightning vertical profiles of Pickering et al. (1998) (C3_PIC) and Ott et al. (2010) (C3).

[Title Page](#)[Abstract](#)[Introduction](#)[Conclusions](#)[References](#)[Tables](#)[Figures](#)[◀](#)[▶](#)[◀](#)[▶](#)[Back](#)[Close](#)[Full Screen / Esc](#)[Printer-friendly Version](#)[Interactive Discussion](#)